

Warm Dark Matter Galaxies with Central Supermassive Black Holes

H. J. de Vega ⁽⁺⁾ and N. G. Sanchez ^(a)

⁽⁺⁾ CNRS LPTHE Sorbonne Université Université Pierre et Marie Curie UPMC Paris, France

^(a) CNRS LERMA PSL Observatoire de Paris Sorbonne Université
and Chalonge - de Vega International School Center, Paris, France.

(Dated: April 26, 2022)

We generalize the Thomas-Fermi approach to galaxy structure to include central supermassive black holes and find selfconsistently and non-linearly the gravitational potential of the galaxy plus the central black hole (BH) system. This approach naturally incorporates the quantum pressure of the fermionic warm dark matter (WDM) particles and shows its full power and clearness in the presence of supermassive black holes. We find the main galaxy and central black hole magnitudes as the halo radius r_h , halo mass M_h , black hole mass M_{BH} , velocity dispersion σ , phase space density, with their realistic astrophysical values, masses and sizes over a wide galaxy range. The supermassive black hole masses arise *naturally* in this framework. Our extensive numerical calculations and detailed analytic resolution of the Thomas-Fermi equations show that in the presence of the central BH **both** DM regimes: classical (Boltzmann dilute) and quantum (compact) do **necessarily** co-exist generically in **any** galaxy: from the smaller and compact galaxies to the largest ones. The ratio $\mathcal{R}(r)$ of the particle wavelength to the average interparticle distance shows consistently that the transition, $\mathcal{R} \simeq 1$, from the quantum to the classical region occurs precisely at **the same point** r_A where the chemical potential vanishes. A **novel halo structure** with three regions shows up: In the vicinity of the BH, WDM is **always** quantum in a small compact core of radius r_A and nearly constant density. In the region $r_A < r < r_i$ till the BH influence radius r_i , WDM is less compact and exhibits a clear classical-Boltzmann like behaviour. For $r > r_i$, the WDM gravity potential dominates and the known halo galaxy shows up with its astrophysical size, DM is a dilute classical gas in this region. As an illustration, three representative families of galaxy plus central BH solutions are found and analyzed: small, medium and large galaxies with realistic supermassive BH masses of $10^5 M_\odot$, $10^7 M_\odot$ and $10^9 M_\odot$ respectively. In the presence of the central BH, we find a *minimum* galaxy size and mass $M_h^{min} \simeq 10^7 M_\odot$, **larger** (2.2233 10^3 times) than the one without BH, and reached at a minimal *non-zero* temperature T_{min} . The supermassive BH **heats-up** the DM and prevents it to become an exactly degenerate gas at zero temperature. Colder galaxies are smaller, warmer galaxies are larger. Galaxies with a central black hole have large masses $M_h > 10^7 M_\odot > M_h^{min}$; compact or ultracompact dwarf galaxies in the range $10^4 M_\odot < M_h < 10^7 M_\odot$ **cannot** harbor central BHs. We find **novel** scaling relations $M_{BH} = DM_h^{\frac{3}{8}}$ and $r_h = CM_{BH}^{\frac{4}{3}}$, and show that the DM galaxy scaling relations: $M_h = b \Sigma_0 r_h^2$, $M_h = a \sigma_h^4 / \Sigma_0$ hold too in the presence of the central BH, Σ_0 being the constant surface density scale over a wide galaxy range. The galaxy equation of state is derived: The pressure $P(r)$ takes huge values in the BH vicinity region and then sharply decreases entering the classical region following consistently a self-gravitating perfect gas $P(r) = \sigma^2 \rho(r)$ behaviour.

(+) : passed away : <https://chalonge-devega.fr/HdeV.html>

(a): <https://chalonge-devega.fr/sanchez/>
Norma.Sanchez@obspm.fr

Contents

I. Introduction and Results	2
II. Galaxy structure with central supermassive black holes in the WDM Thomas-Fermi approach	7
A. Thomas-Fermi equations with a central black hole	8
B. Central Galactic Black Hole and its influence radius	9
C. Main physical magnitudes of the galaxy plus central black hole system	11
D. Galaxy properties in the diluted Boltzmann regime	14
III. Explicit Thomas-Fermi Galaxy solutions with central supermassive black holes	14
A. Local thermal equilibrium in the Galaxy	14
B. Thomas-Fermi equations with r-dependent temperature $T_c(r)$	16
C. Examples of Thomas-Fermi Galaxy solutions with a central supermassive black hole	16

D. Quantum physics in galaxies	18
IV. Systematic study of the Thomas-Fermi Galaxy solutions with a central supermassive black hole	20
A. Universal Scaling relations in the presence of central black holes	22
B. Pressure and equation of state in the presence of central black holes	24
V. Conclusions	24
VI. Appendix. Analytic evaluation of the density and the pressure	32
A. The quantum (high density) regime	32
B. The classical Boltzmann regime	33
References	34

I. INTRODUCTION AND RESULTS

Dark matter (DM) is the main component of galaxies: the fraction of DM over the total galaxy mass goes from 90% for large diluted galaxies till 99.99% for dwarf compact galaxies. Therefore, as a first approximation, DM alone should explain the **main basic magnitudes** of galaxies (as masses and sizes) as well as main structural properties of density profiles and rotation curves. Baryons should give corrections to the pure DM results. For such reasons we consider here Warm Dark Matter galaxies with central supermassive black holes without including baryons as a first approximation.

Warm Dark Matter (WDM), that is dark matter formed by particles with masses of the order of the keV scale receives increasing attention in the last years, (see for example [1], [2], [3], [4], [5], [6], [7], [8], [9], [10], [11], [12], [13], [14], [15], [16], [17], [18] and references therein). At intermediate scales ~ 100 kpc, WDM gives the **correct abundance** of substructures and solves the cold dark matter (CDM) overabundance of structures at small scales [19], [20], [21], [22], [23], [24], [25],[26], [27]. For scales larger than 100 kpc, WDM yields the same results than CDM. Hence, WDM agrees with the small scale as well as large scale structure observations and CMB anisotropy observations.

Astronomical observations show that the DM galaxy density profiles are **cored** till scales below the kpc [28],[29], [30], [31], [32], [33]. On the other hand, N -body CDM simulations exhibit cusped density profiles with a typical $1/r$ behaviour near the galaxy center $r = 0$. Inside galaxy cores, below ~ 100 pc, N -body classical physics simulations do not provide the correct structures for WDM because quantum effects are important in WDM at these scales. Classical that is non quantum physics N -body WDM simulations which do not take into account the quantum WDM pressure exhibit cusps or small cores with sizes smaller than the observed cores [34], [35], [36], [37]. WDM predicts correct structures and cores with the right sizes for small scales (below kpc) when the **quantum** nature of the WDM particles, that is the **quantum pressure** of the fermionic WDM, is taken into account [9], [10],[11],[12].

We follow here the Thomas-Fermi approach to galaxy structure for self-gravitating fermionic WDM [9], [10], [11], [12]. This approach is especially appropriate to take into account quantum properties of systems with large number of particles, namely macroscopic quantum systems as neutron stars, white dwarf stars [38] and galaxies [9], [10],[11], [12].

Fermionic dark matter is appropriate because Dark Matter particles do not interact with the standard or electromagnetic forces, a typical example is the sterile neutrino. Fermionic statistics is totally valid for Dark Matter and the keV Fermionic Dark Matter becomes popular in the last years. The DM particles composing the self-gravitating Fermi gaz only interact through gravitation.

In this paper we generalize the Thomas-Fermi approach to galaxies including their central supermassive black holes.

In this approach, the central quantity to derive is the DM chemical potential $\mu(\mathbf{r})$, which is the free energy per particle. For self-gravitating systems, the potential $\mu(\mathbf{r})$ is proportional to the gravitational potential $\phi(\mathbf{r})$, $\mu(\mathbf{r}) = \mu_0 - m \phi(\mathbf{r})$, μ_0 being a constant, and obeys the **self-consistent** and **nonlinear** Poisson equation

$$\nabla^2 \mu(\mathbf{r}) = -4 \pi g G m^2 \int \frac{d^3 p}{(2 \pi \hbar)^3} f \left(\frac{p^2}{2 m} - \mu(\mathbf{r}) \right). \quad (1.1)$$

Here G is Newton's gravitational constant, g is the number of internal degrees of freedom of the DM particle, m is the DM particle mass, p is the DM particle momentum and $f(E)$ is the energy distribution function. This is a semiclassical gravitational approach to determine selfconsistently the gravitational potential of the quantum fermionic WDM given its distribution function $f(E)$.

In the Thomas-Fermi approach, DM dominated galaxies are considered in a stationary state. This is a realistic situation for the late stages of structure formation since the free-fall (Jeans) time t_{ff} for galaxies is much shorter than the age of galaxies. t_{ff} is at least one or two orders of magnitude smaller than the age of the galaxy.

We consider spherical symmetric configurations where eq.(1.1) becomes an ordinary nonlinear differential equation that determines self-consistently the chemical potential $\mu(r)$ and constitutes the Thomas-Fermi approach [9], [10], [12],[11]. We choose for the energy distribution function a Fermi-Dirac distribution

$$f(E) = \frac{1}{e^{E/T_0} + 1},$$

where T_0 is the characteristic one-particle energy scale. As we see below, except near the central black-hole we can take T_0 constant. T_0 plays the role of an effective temperature scale and depends on the galaxy mass [11], [12].

The Fermi-Dirac distribution function is justified in the inner regions of the galaxy, inside the halo radius where we find that the Thomas-Fermi density profiles perfectly agree with the observations [11], [12]. These results are supported by our work Ref.[13] where within an Eddington-like approach for galaxies, it is shown that the observed galaxy density profiles describe a self-gravitating thermal gas for $r \lesssim R_{virial}$.

Our theoretical results follow by solving the self-consistent and nonlinear Poisson equation eq.(1.1) which is **solely** derived from the purely **gravitational** interaction of the WDM particles and their **fermionic** nature.

The central quantity in the Thomas-Fermi equations (1.1) is the chemical potential $\mu(r)$. The boundary condition of the chemical or gravitational potential $\mu(r)$ at the center $r \rightarrow 0$ in the Thomas-Fermi approach is extended here to allow for the presence of the central black hole, namely,

$$\mu(r) \stackrel{r \rightarrow 0}{\approx} \frac{G m M_{BH}}{r} + Const. + \mathcal{O}(r). \quad (1.2)$$

M_{BH} being the black hole mass. That is, the presence of a galactic central black-hole implies near the center $r \rightarrow 0$, a behavior proportional to $1/r$ in $\mu(r)$, while in the absence of the black-hole let us recall that $\mu(r)$ is bounded for $r \rightarrow 0$ [9], [10], [11], [12].

Positive values of $\mu(r)$ correspond to a self-gravitating quantum gas regime while negative values of $\mu(r)$ describe the self-gravitating classical (Boltzmann) regime [38]. As we see below, one of the results of this paper is that in galaxies possessing central black-holes, **both** regimes do appear. The strong gravitational field of the central black hole makes the WDM chemical potential large and positive near the center. This implies that the WDM behaves **quantum mechanically** inside a small **quantum core** with a nearly constant density.

We summarize in what follows the main results of this paper:

- **(i)** We find that $\mu(r)$ takes large positive values in the inner regions as implied by eq.(2.18), then decreases till vanishing at $r = r_A$, and becomes negative for $r > r_A$, as shown by our detailed resolution of the Thomas-Fermi equation [sec. III C and Fig. 1]. Therefore, r_A is precisely the transition between the quantum and classical DM behaviours, r_A plays the role of the **quantum DM radius** of the galaxy for galaxies exhibiting a central black hole. Namely, inside r_A the WDM gas is a self-gravitating **quantum** gas, while for $r \gtrsim r_A$ the WDM gas is a self-gravitating classical Boltzmann gas. The size r_A of the quantum WDM core turns to be smaller for increasing galaxy masses and black hole masses. WDM inside a small core of radius r_A is in a quantum gas high density state, namely a Fermi nearly degenerate state with nearly constant density ρ_A . For the three representative families of galaxy solutions we find here, the values of r_A and ρ_A are given by eqs.(3.8)-(3.10). The density ρ_A is orders of magnitude larger than its values for $r > r_A$ where the WDM is in the classical Boltzmann regime. r_A runs between 0.07 pc to 1.90 pc for galaxies with virial masses from $10^{16} M_\odot$ to $10^7 M_\odot$ [as shown in sec. III C]. In any case, r_A is much **larger** than the Schwarzschild radius of the central black hole which runs from 10^{-4} pc to 10^{-8} pc.

This is an **important result**: in the vicinity of the central black hole the fermionic WDM is always in a quantum regime while far from the central black hole the WDM follows a classical Boltzmann regime [12]. This is natural to understand: the strong attractive gravitational force near the central BH compacts the WDM and its high density makes it to behave quantum mechanically. On the contrary, far from the BH the gravitational forces are weak, the WDM is diluted and it is then described by a classical Boltzmann gas. Ultracompact dwarf galaxies also exhibit WDM in a quantum regime [9], [10], [12].

- **(ii)** In addition, the black hole has an influence radius r_i . In the vicinity of the black hole, the gravitational force due to the black hole is larger than the gravitational force exercised by the dark matter. The influence radius of the black-hole r_i is defined as the radius where both forces are of equal strength. Both forces point inwards and always sum up. r_i turns to be larger than the radius r_A where the chemical potential vanishes, $r_i > r_A$. The region $r_A < r < r_i$ is dominated by the central black hole and the WDM exhibits there a classical behaviour. For $r \lesssim r_i$, we see from Figs. 1-2 that both $\mu(r)$ and $|d\mu(r)/dr|$, [or equivalently, the dimensionless potential $\nu(\xi)$ and its derivative $|d\nu(\xi)/dx|$, $x = \ln r/r_h$], follow the behaviour dictated by the central black hole eq.(2.22) which produce straight lines on the left part of the logarithmic plots Figs. 1-2. Consistently, for $r \gtrsim r_i$, $\nu(\xi)$ and $|d\nu(\xi)/dx|$ are dominated by the WDM and exhibit a similar behaviour to that of the Thomas-Fermi solutions without a central black hole [9], [10], [11], [12].

Fig. 3 shows that the local density behaviour is dominated by the black hole for $r \lesssim r_i$. For $r_i \lesssim r \lesssim r_h$ the WDM gravitational field dominates over the black hole field and the galaxy core shows up. For medium and large galaxies the core is seen as a plateau. At the same time the chemical potential is negative for $r \gtrsim r_i > r_A$ and the WDM is a classical Boltzmann gas in this region.

The surface density

$$\Sigma_0 \equiv r_h \rho_0 \simeq 120 M_\odot/\text{pc}^2 \quad \text{up to } 10\% - 20\% , \quad (1.3)$$

has the remarkable property of being nearly **constant** and independent of luminosity in different galactic systems (spirals, dwarf irregular and spheroidals, ellipticals) spanning over 14 magnitudes in luminosity and over different Hubble types [32], [31]. It is therefore a useful physical characteristic scale in terms of which express galaxy magnitudes.

- **(iii)** We find the main galaxy magnitudes as the halo radius r_h , halo mass M_h , black hole mass M_{BH} , velocity dispersion, circular velocity, density, pressure and phase space density. Analytic formulae are derived for them and expressed in terms of the reference surface density Σ_0 . Moreover, we can express the black hole mass as

$$M_{BH} = 2.73116 \cdot 10^4 M_\odot \frac{\xi_0}{[\xi_h I_2(\nu_0)]^{\frac{3}{5}}} \left(\frac{\Sigma_0 \text{ pc}^2}{120 M_\odot} \right)^{\frac{3}{5}} \left(\frac{2 \text{ keV}}{m} \right)^{\frac{16}{5}} \quad (1.4)$$

ξ_0 being the dimensionless central radius and $I_2(\nu_0)$ the 2nd momentum of the distribution function eq.(2.11). The black hole mass M_{BH} grows when ξ_0 grows. Notice that M_{BH} does not simply grow linearly with ξ_0 due to the presence of the factor $[\xi_h I_2(\nu_0)]^{-\frac{3}{5}}$.

- **(iv)** We find in this approach explicit realistic galaxy solutions with central supermassive black holes and analyze three representative families of them: Small size (mass) galaxies, intermediate size (mass) galaxies, large size (mass) galaxies.

For a fixed value of the surface density Σ_0 , the solutions are parametrized by two truly physical parameters: the dimensionless central radius ξ_0 and the constant A characteristic of the chemical potential behaviour eq.(2.22) at the center $\xi \rightarrow 0$. The dimensionless central radius ξ_0 is explicitated in Eq.(2.18): This is the ratio of the relevant physical parameters (m, M_{BH}, T) which appear in the chemical potential at the center. The constant A is truly physical too and characterizes the boundary condition of the chemical potential at the center in the presence of the central supermassive black hole, Eq.(2.22). In the absence of the central SMBH: $\xi_0 = 0$, and the boundary condition at the center without BH: $\nu(0) = A$ is recovered.

We derive an illuminating expression for the central radius r_0 for large galaxies $M_h \gtrsim 10^6 M_\odot$ explicitly in terms of the black hole mass M_{BH} , the halo mass M_h and the reference surface density Σ_0 . It follows from eqs.(2.31), (2.33) and (2.56) that,

$$r_0 = l_0 \xi_0 = 126.762 \sqrt{\frac{10^6 M_\odot}{M_h}} \frac{M_{BH}}{10^6 M_\odot} \sqrt{\frac{120 M_\odot}{\Sigma_0 \text{ pc}^2}} \text{ pc} \quad (1.5)$$

- **(v)** We find from our extensive numerical calculations that the halo is thermalized at the uniform temperature T_0 and matches the circular temperature $T_c(r)$ by $r \sim 3 r_h$. This picture is similar to the picture found in the absence of the central black hole which follows from the observed density profiles in the Eddington-like approach to galaxies [13]. We obtain here in the Thomas-Fermi approach and in the presence of a central supermassive black hole that the halo is thermalized at a uniform temperature T_0 inside $r \lesssim 3 r_h$ which tends to the circular

temperature $T_c(r)$ at $r \sim 3 r_h$ as illustrated in Fig. 4. The circular temperature is defined in terms of the circular velocity as: $T_c(r) = \frac{m}{3} v_c^2(r)$. The circular temperature is discussed in Section 3. We introduce the circular Temperature $T_c(r)$ in terms of the circular (virial) velocity $v_c^2(r)$ in the same way the Temperature $T(r)$ is defined in terms of the velocity dispersion $T(r) = mv^2(r)/3$. The circular velocity $v_c^2(r)$ is defined and found in Section 2. Near the central black hole, the space dependent temperature $T_c(r)$ is given by equipartition and the virial theorem, as shown by Eqs. (3.1), (3.2), (3.3).

From our extensive numerical calculations we find that the galaxy mass increases and the galaxy size increases when the constant $|A|$ characteristic of the the central behaviour of $\nu(\xi)$ for $\xi \rightarrow 0$ eq.(2.22) increases. This is similar to the case in the absence of central black holes where $A = \nu(0)$ [9], [10],[12].

- **(vi)** We plot in Fig. 4 the circular velocity given by eq.(2.48) vs. $\log_{10} r/r_h$. For $r > r_h$ the circular velocity tends to the velocity dispersion as obtained from the Eddington equation for realistic density profiles [13]. For $r \rightarrow 0$ the circular velocity grows as in eq.(2.49) due to the central black hole field.
- **(vii)** We find in eqs.(3.8)-(3.10) the WDM mass M_A inside the quantum galaxy radius r_A . M_A represents only a small fraction of the halo or virial mass of the galaxy but it is a significant fraction of the black hole mass M_{BH} . We see from eqs.(3.8)-(3.10) that M_A amounts for 20% of M_{BH} for the medium and large galaxies and 45% for the small galaxy.
- **(viii)** We also measure the classical and quantum gas character of the galaxy plus black hole system by means of the ratio $\mathcal{R}(r)$ between the particle de Broglie wavelength and the average interparticle distance. For $\mathcal{R} \lesssim 1$ the system is of classical dilute nature while for $\mathcal{R} \gtrsim 1$ it is a macroscopic quantum system. We find $\mathcal{R}(r)$ in terms of the surface density and momenta of the gravitational or chemical potential in dimensionless units $\nu(\xi)$ eqs.(3.13), (3.14). Fig. 5 shows $\log_{10} \mathcal{R}$ vs. $\log_{10}(r/r_h)$ for the three representative galaxy solutions. The transition from the quantum to the classical regime occurs precisely at **the same point** r_A where the chemical potential vanishes (see Fig. 1), as it must be, showing the consistency and powerful of our treatment. This point defines the transition from the quantum to the classical behaviour.
- **(ix)** There is an **important qualitative** difference between galaxy solutions with a black hole ($\xi_0 > 0$), and galaxy solutions without a black hole ($\xi_0 = 0$). In the absence of the central black hole, the halo mass M_h reaches the minimal value M_h^{min} Eq. (4.1) which is the degenerate quantum limit at zero temperature $T_0^{min} = 0$ [9], [10], [12]. In the presence of a central black hole, we find that the minimal temperature T_0^{min} is always **non-zero** and that the halo mass takes as minimal value

$$M_h^{min} = 6.892 \cdot 10^7 \left(\frac{2 \text{ keV}}{m} \right)^{\frac{16}{5}} \left(\frac{\Sigma_0 \text{ pc}^2}{120 M_\odot} \right)^{\frac{3}{5}} M_\odot, \text{ with central black hole.} \quad (1.6)$$

$$M_h^{min} = 3.0999 \cdot 10^4 \left(\frac{2 \text{ keV}}{m} \right)^{\frac{16}{5}} \left(\frac{\Sigma_0 \text{ pc}^2}{120 M_\odot} \right)^{\frac{3}{5}} M_\odot, T_0^{min} = 0, \text{ without central black hole.} \quad (1.7)$$

The presence of the supermassive black hole **heats-up** the dark matter gas and prevents it to become an exact degenerate gas at zero temperature. The minimal galaxy mass and size and most compact galaxy state with a central black hole is a nearly degenerate state at very low but non-zero temperature as seen from eq.(4.3). All matter studied in this paper is Dark Matter and the only DM interaction is the gravitational interaction. The presence of the black hole naturally makes the DM particles acquires a higher velocity (and thus a higher associated temperature), and in this sense the SMBH does "heat" the dark matter around it. Gravitation self-consistently, acts on such DM, and the SMBH adds too to such gravitational action. This is a very clean physical process, clean framework and clean conclusive results.

This situation is clearly shown in Fig. 6. The value of M_h^{min} with a central black hole is $2.2233 \cdot 10^3$ times larger than without the black hole. Notice that the small galaxy solution eq.(3.8) is just 11 % larger in halo mass than the minimal galaxy eq.(1.6) with central black hole. **We conclude** that galaxies possessing a central black hole are in the dilute Boltzmann regime because of their large mass $M_h > 10^6 M_\odot > M_h^{min}$ [12]. On the contrary, compact galaxies, in particular ultracompact galaxies in the quantum regime $M_h < 2.3 \cdot 10^6 M_\odot$ [12], **cannot** harbor central black holes because the minimal galaxy mass with central black hole eq.(1.6) is always larger than $2.3 \cdot 10^6 M_\odot$. In other words, galaxies with masses $M_h < M_h^{min}$, namely ultracompact dwarfs **necessarily** do not possess central black holes.

The mass of the supermassive black hole M_{BH} monotonically increases with the central radius r_0 or equivalently the dimensionless one ξ_0 at fixed A . In addition, for $\xi_0 < 0.3$, that is for small supermassive black holes, and all A , the galaxy parameters as halo mass M_h , halo radius r_h , virial mass M_{vir} and galaxy temperature T_0 become **independent** of ξ_0 showing a *limiting galaxy solution*. Only the BH mass depends on ξ_0 in this regime.

Fig. 8 displays our results for the black hole mass $\log_{10} M_{BH}$ vs. the halo mass $\log_{10} M_h$. We see that M_{BH} is a **two-valued** function of M_h . For each value of M_h there are two possible values for M_{BH} which are quite close to each other. This two-valued dependence on M_h is a direct consequence of the dependence of M_h on A shown in Fig. 6. The branch-points on the left in Fig.8, correspond to the minimal galactic halo mass M_h^{min} eq.(4.2) when the central supermassive black hole is present. At **fixed** ξ_0 , as shown in Fig. 8, the central black hole mass M_{BH} **scales** with the halo mass M_h as

$$M_{BH} = D(\xi_0) M_h^{\frac{3}{8}},$$

where $D(\xi_0)$ is an increasing function of ξ_0 . We plot in Fig. 9 the halo galaxy mass $\log_{10} M_h$ vs. the galaxy temperature $\log_{10} T_0/\text{K}$. The halo mass M_h grows when T_0 increases. Colder galaxies are smaller. Warmer galaxies are larger. We see at the branch-points in Fig. 9 the minimal galaxy temperature T_0^{min} eq.(4.3) when a supermassive black hole is present.

We find galaxy solutions with central black holes for arbitrarily small values of $\xi_0 > 0$ and correspondingly arbitrarily small central BH mass. There is no minimal central BH mass. The only minimal central BH mass possibility is zero (for $\xi = 0$).

- **(x)** We find that M_h **scales** as r_h^2 , which is the same scaling found in the Thomas-Fermi approach to galaxies in the absence of black holes [9], [10], [12]. We plot in Fig. 10 the ordinary logarithm of the halo radius $\log_{10} r_h$ vs. the ordinary logarithm of the halo mass $\log_{10} M_h$ for galaxies with central black holes of many different masses. The halo mass in the absence of a central black hole behaves in the Thomas-Fermi approach as [12]

$$M_h = 1.75572 \Sigma_0 r_h^2, \quad \text{without central black hole.} \quad (1.8)$$

The proportionality factor in this scaling relation is confirmed by the galaxy data [12]. In the presence of a central black hole we find in the Thomas-Fermi approach an analogous relation

$$M_h = b \Sigma_0 r_h^2, \quad \text{with central black hole.} \quad (1.9)$$

where the coefficient b turns to be of order unity. We plot in Fig.11 the coefficient b as a function of the halo mass M_h . We see that except for halo masses near the minimum halo mass M_h^{min} , b in the presence of a central black hole takes values up to 10% below its value in the absence of a central black hole eq.(4.4). For halo masses near M_h^{min} , b increases reaching values $b \leq 4$. For very large halos and central black holes, b could be as small as about 1.6. b changes at most by a factor from 1/2 up to 2 while the halo mass M_h varies ten orders of magnitude. As shown by Fig.11, b is a two-valued function of M_h . b turns to be independent of the precise value of the WDM particle mass m , which is due to the fact that the scaling relation eq.(4.5) as well as eq.(4.4) apply in the classical Boltzmann regime of the galaxy ($M_h \gtrsim 10^6 M_\odot$). **In summary**, the scaling relation eq.(4.5) and the coefficient b turn out to be **remarkably robust**.

- **(xi)** We plot in Fig. 12 the ordinary logarithm of the halo radius $\log_{10} r_h$ versus the ordinary logarithm of the central black hole mass $\log_{10} M_{BH}$ for many galaxy solutions. The halo radius r_h turns to be a double-valued function of M_{BH} . Remarkably, r_h for **fixed** ξ_0 scales as

$$r_h = C(\xi_0) M_{BH}^{\frac{4}{3}}. \quad (1.10)$$

The constant $C(\xi_0)$ turns to be a decreasing function of ξ_0 .

- **(xii)** We find the local pressure $P(r)$ as given by eq. (2.43). In Fig.13 we plot $\log_{10} P(r)$ vs. $\log_{10}(r/r_h)$ for the three representative galaxy solutions. $P(r)$ monotonically decreases with r . The pressure $P(r)$ takes huge values in the quantum (high density) region $r < r_A$ and then it sharply decreases entering the classical (dilute) region $r > r_A$. In Fig.14 we plot the derived **equation of state** $\log_{10} P(r)$ vs. $\log_{10} \rho(r)/\rho_0$ for the three galaxy solutions we find here with central SMBH. The three curves almost coincide and are almost straight lines of unit slope. That is, the equation of state is in very good approximation a perfect gas equation of state $P(r) = \sigma^2 \rho(r)$, which stems from the fact that galaxies with central black holes have halo masses $M_h > M_h \gtrsim 10^6 M_\odot > M_h^{min}$ eq.(4.2) and therefore necessarily belong to the *dilute* Boltzmann classical regime [12]. The equation of state turns out to be a local (r -dependent) perfect gas equation of state because of the gravitational interaction,

(WDM self-gravitating perfect gas). Indeed, for galaxies with central black holes the WDM is in a quantum (highly compact) regime inside the quantum radius r_A . However, because r_A is in the parsec scale or smaller [see eqs.(3.8)-(3.10)] the bulk of the WDM is in the Boltzmann classical regime which is consistently reflected in the perfect gas equation of state behaviour.

In summary, the results of this paper show the power and cleanliness of the Thomas-Fermi theory and WDM to properly describe the galaxy structures and the galaxy physical states with and without supermassive central black holes. We consider in this paper pure WDM galaxies with central supermassive black holes. Adding baryons will introduce corrections, but the picture of galaxies with central supermassive black holes presented here should not change essentially. This approach is **independent** of any WDM particle physics model. It depends only of the fermionic WDM nature and gravity. The results presented in this paper do not depend on the precise value of the WDM particle mass m but only on the fact that m is in the keV scale, namely $keV \lesssim m \lesssim 10 keV$ say.

This paper is organized as follows:

In Section II we formulate the problem of galaxy structure with central supermassive black holes in the WDM Thomas-Fermi approach and find the main physical magnitudes and properties of the galaxy plus black hole system. In Section III we solve the corresponding equations with the boundary conditions, find three representative families of galaxy solutions (small, medium and large size galaxies) with central supermassive black holes and analyze the new quantum and classical physics properties of the system. In Section IV we perform an extensive study of the galaxy solutions with a central supermassive black hole, find the main important differences between galaxies with and without the presence of a central black hole, derive universal galaxy scaling relations in the presence of a central supermassive black hole: halo mass M_h - halo size r_h relation, black hole mass M_{BH} - halo radius r_h relation, and find the galaxy local pressure and equation of state in the presence of central supermassive black holes and their different regimes.

II. GALAXY STRUCTURE WITH CENTRAL SUPERMASSIVE BLACK HOLES IN THE WDM THOMAS-FERMI APPROACH

We consider DM dominated galaxies in their late stages of structure formation when they are relaxing to a stationary situation, at least not too far from the galaxy center.

This is a realistic situation since the free-fall (Jeans) time t_{ff} for galaxies is much shorter than the age of galaxies:

$$t_{ff} = \frac{1}{\sqrt{G \rho_0}} = 1.49 \cdot 10^7 \sqrt{\frac{M_\odot}{\rho_0 \text{ pc}^3}} \text{ yr} . \quad (2.1)$$

The observed central densities of galaxies yield free-fall times in the range from 15 million years for ultracompact galaxies till 330 million years for large diluted spiral galaxies. These free-fall (or collapse) times are small compared with the age of galaxies running in billions of years.

Hence, we can consider the DM described by a time independent and energy distribution function $f(E)$, where $E = \sqrt{p^2 + m^2} - m - \mu$ is the *relativistic* single-particle energy, m is the mass of the DM particle and μ is the chemical potential [9], [10], [12] related to the gravitational potential $\phi(\mathbf{r})$ by

$$\mu(\mathbf{r}) = \mu_0 - m \phi(\mathbf{r}) , \quad (2.2)$$

where μ_0 is a constant. We consider here *relativistic* kinematics because the WDM particles in the vicinity of the central black hole can be relativistic. In the non-relativistic limit we recover the relations used in Refs. [9], [10], [12].

In the Thomas-Fermi approach, $\rho(\mathbf{r})$ is expressed as a function of $\mu(\mathbf{r})$ through the standard integral of the DM phase-space distribution function over the momentum

$$\rho(\mathbf{r}) = \frac{g}{2 \pi^2 \hbar^3} \int_0^\infty dp p^2 \sqrt{p^2 + m^2} f \left[\sqrt{p^2 + m^2} - m - \mu(\mathbf{r}) \right] , \quad (2.3)$$

where g is the number of internal degrees of freedom of the DM particle, with $g = 1$ for Majorana fermions and $g = 2$ for Dirac fermions. Eq.(2.3) is valid in general for relativistic fermions and *generalizes* the non-relativistic framework of refs. [9], [10], [12].

We will consider spherical symmetric configurations. Then, the Poisson equation for $\phi(r)$ takes the self-consistent form

$$\frac{d^2\mu}{dr^2} + \frac{2}{r} \frac{d\mu}{dr} = -4\pi G m \rho(r) = -\frac{2g G m}{\pi \hbar^3} \int_0^\infty dp p^2 \sqrt{p^2 + m^2} f \left[\sqrt{p^2 + m^2} - m - \mu(r) \right], \quad (2.4)$$

where G is Newton's constant and $\rho(r)$ is the DM mass density.

Eq. (2.4) provides an ordinary **nonlinear** differential equation that determines **self-consistently** the chemical potential $\mu(r)$ and constitutes the Thomas-Fermi approach [9], [10], [12] (see also ref. [39]). This is a semi-classical approach to galaxy structure in which the quantum nature of the DM particles is taken into account through the quantum statistical distribution function $f(E)$.

The DM pressure and the velocity dispersion can also be expressed as integrals over the DM phase-space distribution function as

$$P(r) = \frac{1}{3} \rho(r) \langle v^2(r) \rangle = \frac{g}{6 \pi^2 \hbar^3} \int_0^\infty dp \frac{p^4}{\sqrt{p^2 + m^2}} f \left[\sqrt{p^2 + m^2} - m - \mu(r) \right], \quad (2.5)$$

We see that $\mu(r)$ fully characterizes the DM halo structure in this Thomas-Fermi framework.

In this semi-classical framework the stationary energy distribution function $f(E)$ must be given. We consider the Fermi-Dirac distribution

$$f(E) = \Psi_{\text{FD}}(E/T_0) = \frac{1}{e^{E/T_0} + 1}, \quad (2.6)$$

where the characteristic one-particle energy scale T_0 in the DM halo plays the role of an effective temperature. T_0 can be taken constant except near the central black hole.

In neutron stars, where the neutron mass is about six orders of magnitude larger than the WDM particle mass, the temperature can be approximated by zero.

As shown in ref. [12], the value of T_0 depends on the galaxy mass. In galaxies, $T_0 \sim m \langle v^2 \rangle$ turns to be non-zero but small in the range: $10^{-3} \text{ K} \lesssim T_0 \lesssim 10 \text{ K}$ for all halo galaxy masses in the range $10^5 - 10^{12} M_\odot$ which reproduce the observed velocity dispersions for $m \simeq 2 \text{ keV}$. The smaller values of T_0 correspond to compact dwarf galaxies and the larger values of T_0 are for large and diluted galaxies [12].

More precisely, large positive values of the chemical potential correspond to the degenerate fermions limit which is the extreme quantum state, and oppositely, large negative values of the chemical potential at the origin give the diluted states which are in the classical regime. The quantum degenerate regime describes dwarf and compact galaxies while the classical diluted regime describes large and diluted galaxies. In the classical regime, the Thomas-Fermi equation (2.4) become the equations for a self-gravitating Boltzmann gas.

Galaxies possessing central black holes exhibit *both* quantum and classical regions as we see below.

The units used in this paper are those appropriate to the keV mass of the dark matter particle in the context of galaxy structure. The expression and conversion of units in terms of the keV includes the Planck constant h . Relevant conversion relations in terms of keV in this context are

$$keV \text{ kpc} = 1,563738 \cdot 10^{29} \quad (2.7)$$

$$M_\odot = 1,115468 \cdot 10^{63} \text{ keV} \quad (2.8)$$

A. Thomas-Fermi equations with a central black hole

It is useful to introduce dimensionless variables ξ , $\nu(\xi)$

$$r = l_0 \xi \quad , \quad \mu(r) = T_0 \nu(\xi) \quad , \quad f(E) = \Psi(E/T_0), \quad (2.9)$$

where l_0 is the characteristic length that emerges from the dynamical equation (2.4):

$$l_0 \equiv \frac{\hbar}{\sqrt{8G}} \left(\frac{2}{g} \right)^{\frac{1}{3}} \left[\frac{9\pi I_2(\nu_0)}{m^8 \rho_0} \right]^{\frac{1}{6}} = R_0 \left(\frac{2 \text{ keV}}{m} \right)^{\frac{4}{3}} \left(\frac{2}{g} \right)^{\frac{1}{3}} \left[\frac{I_2(\nu_0)}{\rho_0} \frac{M_\odot}{\text{pc}^3} \right]^{\frac{1}{6}}, \quad R_0 = 7.425 \text{ pc}, \quad (2.10)$$

and

$$I_2(\nu) \equiv 3 \int_0^\infty y^2 dy \sqrt{1 + \frac{2y^2}{\tau}} \Psi_{FD} \left(\tau \left[\sqrt{1 + \frac{2y^2}{\tau}} - 1 \right] - \nu \right), \quad (2.11)$$

$$\tau \equiv \frac{m}{T_0}, \quad \nu_0 \equiv \nu(\xi_i), \quad \rho_0 = \rho(\xi_i) \quad (2.12)$$

where we use the integration variable $y \equiv p/\sqrt{2mT_0}$. ξ_i stands for the influence radius of the black hole which is defined below by eq.(2.21).

We consider in eq.(2.11) the case of a constant temperature T_0 . The case of a r -dependent temperature is analysed in sec. III B.

For definiteness, we will take $g = 2$, Dirac fermions in the sequel. One can easily translate from Dirac to Majorana fermions changing the WDM fermion mass as:

$$m \Rightarrow \frac{m}{2^{\frac{1}{4}}} = 0.8409 m .$$

Then, in dimensionless variables, the self-consistent Thomas-Fermi equation (2.4) for the chemical potential $\nu(\xi)$ takes the form

$$\frac{d^2\nu}{d\xi^2} + \frac{2}{\xi} \frac{d\nu}{d\xi} = -I_2(\nu) \quad . \quad (2.13)$$

The presence of the central black hole is introduced through the boundary conditions eq.(2.22) given below for the chemical potential $\nu(\xi)$ at $\xi \rightarrow 0$.

B. Central Galactic Black Hole and its influence radius

In the presence of a central galactic black hole the gravitational potential and the chemical potential near the center take the form

$$\phi(r) \stackrel{r \rightarrow 0}{\approx} -\frac{G M_{BH}}{r}, \quad \mu(r) - \mu_0 \stackrel{r \rightarrow 0}{\approx} \frac{G m M_{BH}}{r}, \quad (2.14)$$

where M_{BH} is the black hole mass.

Integrating eq.(2.4) from $r = 0$ to r yields

$$r^2 \frac{d\mu}{dr} - \left[r^2 \frac{d\mu}{dr} \Big|_{r \rightarrow 0} \right] = -G m M(r) \quad (2.15)$$

where

$$M(r) = 4\pi \int_0^r dr' r'^2 \rho(r'). \quad (2.16)$$

is the total WDM mass $M(r)$ enclosed in a sphere of radius r not including the central black hole mass.

Inserting the $r \rightarrow 0$ behaviour eq. (2.14) into eq. (2.15) yields for the derivative of the chemical potential

$$\frac{d\mu}{dr} = -\frac{G m}{r^2} [M(r) + M_{BH}], \quad (2.17)$$

showing that the chemical potential is monotonically decreasing in r .

From eqs.(2.2) and (2.9) the dimensionless chemical potential $\nu(\xi)$ takes the form

$$\nu(\xi) \stackrel{\xi \rightarrow 0}{\approx} \frac{G m M_{BH}}{T_0 l_0 \xi} \equiv \frac{\xi_0}{\xi} = \frac{r_0}{r}, \quad \xi_0 \equiv \frac{G m M_{BH}}{T_0 l_0} = \frac{r_0}{l_0}. \quad (2.18)$$

That is, the presence of a galactic central black hole implies near the center $\xi \rightarrow 0$, a ξ_0/ξ behavior in $\nu(\xi)$. ξ_0 is proportional to the black hole mass M_{BH} . Recall that in the absence of the black hole $\nu(\xi)$ is bounded for $\xi \rightarrow 0$ [9, 10, 12].

We see from eq.(2.18) that in the vicinity $\xi \lesssim \xi_0$ of the central black hole, the chemical potential $\nu(\xi)$ is dominated by its boundary expression eq.(2.18) and therefore $\nu(\xi)$ takes positive values $\nu(\xi) \gtrsim 1$. Values of $\nu(\xi)$ larger than unity correspond to a fermionic WDM gas in a quantum regime [38]. This is an **important result**: in the vicinity of the central black hole the fermionic WDM is always in a quantum regime while far from the central black hole the WDM follows a classical Boltzmann regime [12]. This is natural to understand: the strong attractive gravitational force near the central BH compacts the WDM and its high density makes it to behave quantum mechanically. On the contrary, far from the BH the gravitational forces are weak, the WDM is diluted and it is then described by a classical Boltzmann gas.

Ultracompact dwarf galaxies also exhibit WDM in a quantum regime [9], [10], [12].

$\nu(\xi)$ takes large positive values for $\xi \ll \xi_0$ as implied by eq.(2.18), then decreases till vanishing at $\xi = \xi_A$, $\nu(\xi_A) = 0$ and becomes negative for $\xi > \xi_A$, as shown by our detailed resolution of the Thomas-Fermi equation [sec. III C and Fig. 1].

Therefore, $r_A = l_0 \xi_A$ plays the role of the **quantum DM radius** of the galaxy for galaxies exhibiting a central black hole. Namely, inside r_A the WDM gas is a **quantum** gas, while for $r \gtrsim r_A$ the WDM gas is a classical Boltzmann gas.

That is, a small **quantum core** of DM forms around the central black hole. The size r_A of the quantum core turns to be smaller for increasing galaxy masses and black-hole masses because the larger is the black hole mass, the larger is its gravitational attraction on the WDM which is thus more compact and hence smaller is the quantum radius core r_A .

r_A runs between 0.07 pc to 1.90 pc for galaxies with virial masses from $10^{16} M_\odot$ to $10^7 M_\odot$ [see sec. III C]. In any case, r_A is much **larger** than the Schwarzschild radius of the central black hole which runs from 10^{-4} pc to 10^{-8} pc.

In the vicinity of the black hole, the gravitational force due to the black hole is larger than the gravitational force exerted by the dark matter. The influence radius of the black hole r_i is defined as the radius where both forces are of equal strength. Notice, that both forces point inwards and always sum up.

The total gravitational potential $V(r)$ and its derivative $V'(r)$ are given by

$$V(r) = -\frac{G M_{BH}}{r} + \phi(r) \quad , \quad V'(r) = \frac{G M_{BH}}{r^2} - \frac{1}{m} \mu'(r) \quad (2.19)$$

where we used eq.(2.2). In dimensionless variables $V'(r)$ becomes

$$V'(r) = \frac{T_0}{m l_0 \xi} \left[\frac{\xi_0}{\xi} - \xi \frac{d\nu}{d\xi} \right] \quad (2.20)$$

The black hole and dark matter gravitational forces become equal at $\xi = \xi_i$. ξ_i is the solution of the equation

$$\xi_i^2 \left. \frac{d\nu}{d\xi} \right|_{\xi_i} = \xi_0 \quad (2.21)$$

In the Thomas-Fermi approach to galaxies with a central supermassive black hole, the boundary condition for $\nu(\xi)$ at $\xi \rightarrow 0$ imposes the black hole presence according to eq.(2.18). That is,

$$\nu(\xi) \stackrel{\xi \rightarrow 0}{\simeq} \frac{\xi_0}{\xi} + A + \mathcal{O}(\xi) \quad (2.22)$$

where ξ_0 is the dimensionless radius defined in eq.(2.18) and A is a constant that determines the properties of the corresponding galaxy solution as the galaxy mass and galaxy radius. In the absence of the central BH, we have $\xi_0 = 0$, $\nu(0) = A$ and the boundary condition used in refs. [9], [10], [12] is recovered.

C. Main physical magnitudes of the galaxy plus central black hole system

We find the main physical galaxy magnitudes, such as the mass density $\rho(r)$, the velocity dispersion $\sigma^2(r) = v^2(r)/3$ and the pressure $P(r)$, which are all r -dependent, as:

$$\rho(r) = \frac{m^{\frac{5}{2}}}{3 \pi^2 \hbar^3} (2 T_0)^{\frac{3}{2}} I_2(\nu(\xi)) = \rho_0 \frac{I_2(\nu(\xi))}{I_2(\nu_0)}, \quad \rho_0 = \frac{m^{\frac{5}{2}}}{3 \pi^2 \hbar^3} (2 T_0)^{\frac{3}{2}} I_2(\nu_0) \quad (2.23)$$

$$P(r) = \frac{m^{\frac{3}{2}}}{15 \pi^2 \hbar^3} (2 T_0)^{\frac{5}{2}} I_4(\nu(\xi)) = \frac{1}{5} (9 \pi^4)^{\frac{1}{3}} \left(\frac{\hbar^6}{m^8} \right)^{\frac{1}{3}} \left[\frac{\rho_0}{I_2(\nu_0)} \right]^{5/3} I_4(\nu(\xi)) \quad (2.24)$$

$$I_4(\nu) \equiv 5 \int_0^\infty \frac{y^4 dy}{\sqrt{1 + \frac{2y^2}{\tau}}} \Psi_{FD} \left(\tau \left[\sqrt{1 + \frac{2y^2}{\tau}} - 1 \right] - \nu \right). \quad (2.25)$$

As a consequence, from eqs.(2.17), (2.9), (2.10), and (2.23) the total WDM mass $M(r)$ enclosed in a sphere of radius r (not including the central black hole mass) turns to be

$$M(r) = 4 \pi \frac{\rho_0 l_0^3}{I_2(\nu_0)} \int_0^\xi dx x^2 I_2(\nu(x)). \quad (2.26)$$

That is, $M(r)$ is the mass enclosed inside a sphere of radius r not including the mass of the central black hole mass.

The integral eq.(2.26) can be computed in closed form by integrating both sides of eq.(2.13)

$$M(r) = 4 \pi \frac{\rho_0 l_0^3}{I_2(\nu_0)} \left\{ \xi^2 |\nu'(\xi)| - \left[\xi^2 |\nu'(\xi)| \right]_{\xi \rightarrow 0} \right\} \quad (2.27)$$

The contribution here from $\xi \rightarrow 0$ is obtained from the boundary condition eq.(2.22) with the result

$$\begin{aligned} M(r) &= M_0 \xi^2 |\nu'(\xi)| \left(\frac{\text{keV}}{m} \right)^4 \sqrt{\frac{\rho_0}{I_2(\nu_0)} \frac{\text{pc}^3}{M_\odot}} - M_{BH}, \\ M_0 &= 4 \pi M_\odot \left(\frac{R_0}{\text{pc}} \right)^3 = 0.8230 \cdot 10^5 M_\odot. \end{aligned} \quad (2.28)$$

In absence of the central black hole we recover the expression for the total mass $M(r)$ obtained in ref. [12].

In these expressions, we have systematically eliminated the energy scale T_0 in terms of the central density ρ_0 through eq.(2.23).

We define the core size r_h of the halo by analogy with the Burkert density profile as

$$\frac{\rho(r_h)}{\rho_0} = \frac{1}{4}, \quad r_h = l_0 \xi_h. \quad (2.29)$$

It must be noticed that the surface density

$$\Sigma_0 \equiv r_h \rho_0, \quad (2.30)$$

is found nearly **constant** and independent of luminosity in different galactic systems (spirals, dwarf irregular and spheroidals, ellipticals) spanning over 14 magnitudes in luminosity and over different Hubble types. More precisely, all galaxies seem to have the same value for Σ_0 , namely $\Sigma_0 \simeq 120 M_\odot/\text{pc}^2$ up to 10% – 20% [31–33]. It is remarkable that at the same time other important structural quantities as r_h , ρ_0 , the baryon-fraction and the galaxy mass vary orders of magnitude from one galaxy to another.

The constancy of Σ_0 seems unlikely to be a mere coincidence and probably reflects a physical scaling relation between the mass and halo size of galaxies. It must be stressed that Σ_0 is the only dimensionful quantity which is practically constant among the different galaxies.

It is then useful to take here the dimensionful quantity Σ_0 as physical scale to express the galaxy magnitudes in the Thomas-Fermi approach. That is, we replace the central density ρ_0 in the above galaxy magnitudes eqs.(2.10)-(2.28) in terms of Σ_0 eq.(2.30) with the following results

$$l_0 = \left(\frac{9 \pi}{2^9} \right)^{\frac{1}{5}} \left(\frac{\hbar^6}{G^3 m^8} \right)^{\frac{1}{5}} \left[\frac{\xi_h I_2(\nu_0)}{\Sigma_0} \right]^{\frac{1}{5}}, \quad (2.31)$$

$$l_0 = 4.2557 [\xi_h I_2(\nu_0)]^{\frac{1}{5}} \left(\frac{2 \text{ keV}}{m} \right)^{\frac{3}{5}} \left(\frac{120 M_\odot}{\Sigma_0 \text{ pc}^2} \right)^{\frac{1}{5}} \text{ pc}$$

$$T_0 = \left(18 \pi^6 \frac{\hbar^6 G^2}{m^3} \right)^{\frac{1}{5}} \left[\frac{\Sigma_0}{\xi_h I_2(\nu_0)} \right]^{\frac{4}{5}}, \quad (2.32)$$

$$T_0 = \frac{7.12757 \cdot 10^{-3}}{[\xi_h I_2(\nu_0)]^{\frac{4}{5}}} \left(\frac{2 \text{ keV}}{m} \right)^{\frac{3}{5}} \left(\frac{\Sigma_0 \text{ pc}^2}{120 M_\odot} \right)^{\frac{4}{5}} \text{ K}.$$

The dimensionless quantum radius of the galaxie ξ_0 eq.(2.18) can be expressed as

$$\xi_0 = \left(\frac{2^8}{3^4 \pi^7} \right)^{\frac{1}{5}} \left[\frac{\xi_h I_2(\nu_0)}{\Sigma_0} \right]^{\frac{3}{5}} G^{\frac{6}{5}} m^{\frac{16}{5}} M_{BH}, \quad (2.33)$$

$$\xi_0 = 36.6145 \left[\xi_h I_2(\nu_0) \frac{120 M_\odot}{\Sigma_0 \text{ pc}^2} \right]^{\frac{3}{5}} \left(\frac{m}{2 \text{ keV}} \right)^{\frac{16}{5}} \frac{M_{BH}}{10^6 M_\odot}. \quad (2.34)$$

Moreover, we can express from here the black hole mass as

$$M_{BH} = 2.73116 \cdot 10^4 M_\odot \frac{\xi_0}{[\xi_h I_2(\nu_0)]^{\frac{3}{5}}} \left(\frac{\Sigma_0 \text{ pc}^2}{120 M_\odot} \right)^{\frac{3}{5}} \left(\frac{2 \text{ keV}}{m} \right)^{\frac{16}{5}}. \quad (2.35)$$

Furthermore, we get

$$r = 4.2557 \xi [\xi_h I_2(\nu_0)]^{\frac{1}{5}} \left(\frac{2 \text{ keV}}{m} \right)^{\frac{3}{5}} \left(\frac{120 M_\odot}{\Sigma_0 \text{ pc}^2} \right)^{\frac{1}{5}} \text{ pc} \quad (2.36)$$

$$\rho(r) = \left(\frac{2^9 G^3 m^8}{9 \pi \hbar^6} \right)^{\frac{1}{5}} \left[\frac{\Sigma_0}{\xi_h I_2(\nu_0)} \right]^{\frac{6}{5}} I_2(\nu(\xi)), \quad (2.37)$$

$$\rho(r) = 18.1967 ; \frac{I_2(\nu(\xi))}{[\xi_h I_2(\nu_0)]^{\frac{6}{5}}} \left(\frac{m}{2 \text{ keV}} \right)^{\frac{3}{5}} \left(\frac{\Sigma_0 \text{ pc}^2}{120 M_\odot} \right)^{\frac{6}{5}} \frac{M_\odot}{\text{pc}^3} \quad (2.38)$$

$$M(r) + M_{BH} = 4 \pi \left(\frac{9 \pi \hbar^6}{2^9 G^3 m^8} \right)^{\frac{2}{5}} \left[\frac{\Sigma_0}{\xi_h I_2(\nu_0)} \right]^{\frac{3}{5}} \xi^2 |\nu'(\xi)|, \quad (2.39)$$

$$M(r) + M_{BH} = \frac{27312 \xi^2}{[\xi_h I_2(\nu_0)]^{\frac{3}{5}}} |\nu'(\xi)| \left(\frac{2 \text{ keV}}{m} \right)^{\frac{16}{5}} \left(\frac{\Sigma_0 \text{ pc}^2}{120 M_\odot} \right)^{\frac{3}{5}} M_\odot \quad (2.40)$$

$$\sigma^2(r) = \frac{1}{3} v^2(r) = \frac{11.0402}{[\xi_h I_2(\nu_0)]^{\frac{4}{5}}} \frac{I_4(\nu(\xi))}{I_2(\nu(\xi))} \left(\frac{2 \text{ keV}}{m} \right)^{\frac{8}{5}} \left(\frac{\Sigma_0 \text{ pc}^2}{120 M_\odot} \right)^{\frac{4}{5}} \left(\frac{\text{km}}{\text{s}} \right)^2, \quad (2.41)$$

$$P(r) = \frac{8\pi}{5} G \left[\frac{\Sigma_0}{\xi_h I_2(\nu_0)} \right]^2 I_4(\nu(\xi)), \quad (2.42)$$

$$P(r) = \frac{200.895}{[\xi_h I_2(\nu_0)]^2} I_4(\nu(\xi)) \left(\frac{\Sigma_0 \text{ pc}^2}{120 M_\odot} \right)^2 \frac{M_\odot}{\text{pc}^3} \left(\frac{\text{km}}{\text{s}} \right)^2. \quad (2.43)$$

That is, $M(r) + M_{BH}$ is the total mass inside a sphere of radius r including the mass of the central black hole.

Notice that both $M(r)$ and M_{BH} at fixed Σ_0 *do scale* with the WDM particle mass as $m^{-\frac{16}{5}}$.

In particular, the halo galaxy mass M_h follows from eq.(2.40) at $r = r_h$:

$$M_h \equiv M(r_h) + M_{BH} = \frac{27312 \xi_h^{\frac{7}{5}}}{[I_2(\nu_0)]^{\frac{3}{5}}} |\nu'(\xi_h)| \left(\frac{2 \text{ keV}}{m} \right)^{\frac{16}{5}} \left(\frac{\Sigma_0 \text{ pc}^2}{120 M_\odot} \right)^{\frac{3}{5}} M_\odot. \quad (2.44)$$

The phase-space density $Q(r)$ follows from eqs.(2.38) and (2.41) as

$$Q(r) \equiv \frac{\rho(r)}{\sigma^3(r)} = 3 \sqrt{3} \frac{\rho(r)}{\langle v^2 \rangle^{\frac{3}{2}}(r)} = \frac{\sqrt{125}}{3 \pi^2} \frac{m^4}{\hbar^3} \frac{I_2^{\frac{5}{2}}(\nu(\xi))}{I_4^{\frac{3}{2}}(\nu(\xi))}. \quad (2.45)$$

Notice that $Q(r)$ turns to be independent of T_0 and Σ_0 . In addition, $Q(r)/m^4$ has no explicit dependence on the DM particle mass.

For a fixed value of the surface density Σ_0 , the solutions of the Thomas-Fermi eqs.(2.13) are parametrized by two parameters: the dimensionless central radius ξ_0 and the constant A characteristic of the chemical potential behaviour eq.(2.22) at the center $\xi \rightarrow 0$.

Also, at fixed surface density Σ_0 , the halo mass M_h , the black hole mass M_{BH} , the characteristic length l_0 , the density ρ_0 and the effective temperature T_0 are only functions of ξ_0 and the constant A .

The circular velocity $v_c(r)$ is defined through the virial theorem as

$$v_c(r) \equiv \sqrt{\frac{G [M(r) + M_{BH}]}{r}}, \quad (2.46)$$

and it is directly related by eq.(2.17) to the derivative of the chemical potential as

$$v_c(r) = \sqrt{-\frac{r}{m} \frac{d\mu}{dr}} = \sqrt{-\frac{T_0}{m} \frac{d\nu}{d \ln \xi}}. \quad (2.47)$$

Expressing T_0 in terms of the surface density Σ_0 using eq.(2.32) we have for the circular velocity the explicit expression

$$v_c(r) = 5.2537 \frac{\sqrt{-\xi \nu'(\xi)}}{[\xi_h I_2(\nu_0)]^{\frac{2}{5}}} \left(\frac{2 \text{ keV}}{m} \right)^{\frac{4}{5}} \left(\frac{\Sigma_0 \text{ pc}^2}{120 M_\odot} \right)^{\frac{2}{5}} \frac{\text{km}}{\text{s}}. \quad (2.48)$$

For $r \rightarrow 0$ the circular velocity $v_c(r)$ grows due to the black hole field as

$$v_c(r) \stackrel{r \rightarrow 0}{\approx} \sqrt{\frac{T_0}{m} \frac{r_0}{r}}, \quad (2.49)$$

where we used eqs.(2.14) and (2.47).

D. Galaxy properties in the diluted Boltzmann regime

In the diluted Boltzmann regime, $\nu_0 \lesssim -5$ corresponding to large galaxies $M_h \gtrsim 10^6 M_\odot$, we find for the main galaxy magnitudes the following analytic expressions:

$$M_h = 1.75572 \Sigma_0 r_h^2 \quad , \quad r_h = 68.894 \sqrt{\frac{M_h}{10^6 M_\odot} \frac{120 M_\odot}{\Sigma_0 \text{ pc}^2}} \text{ pc} \quad (2.50)$$

$$T_0 = 8.7615 \cdot 10^{-3} \sqrt{\frac{M_h}{10^6 M_\odot}} \frac{m}{2 \text{ keV}} \sqrt{\frac{\Sigma_0 \text{ pc}^2}{120 M_\odot}} \text{ K} \quad (2.51)$$

$$\rho(r) = 5.19505 \left(\frac{M_h}{10^4 M_\odot} \frac{\Sigma_0 \text{ pc}^2}{120 M_\odot} \right)^{\frac{3}{4}} \left(\frac{m}{2 \text{ keV}} \right)^4 e^{\nu(\xi)} \frac{M_\odot}{\text{pc}^3} \quad (2.52)$$

$$v_c^2(r) = 33.9297 \sqrt{\frac{M_h}{10^6 M_\odot} \frac{\Sigma_0 \text{ pc}^2}{120 M_\odot}} \left| \frac{d\nu(\xi)}{d \ln \xi} \right| \left(\frac{\text{km}}{\text{s}} \right)^2 \quad , \quad (2.53)$$

$$v_c^2(r_h) = 62.4292 \sqrt{\frac{M_h}{10^6 M_\odot} \frac{\Sigma_0 \text{ pc}^2}{120 M_\odot}} \left(\frac{\text{km}}{\text{s}} \right)^2 \quad (2.54)$$

$$M(r) + M_{BH} = 7.88895 \left| \frac{d\nu(\xi)}{d \ln \xi} \right| \frac{r}{\text{pc}} \sqrt{\frac{M_h}{10^6 M_\odot} \frac{\Sigma_0 \text{ pc}^2}{120 M_\odot}} \quad (2.55)$$

Eqs.(2.32) and (2.51) allow us to express the quantity $\xi_h I_2(\nu_0)$ in terms of the observable galaxy magnitudes M_h and Σ_0 for large galaxies $M_h \gtrsim 10^6 M_\odot$ in the diluted regime. We obtain from eqs.(2.32) and (2.51)

$$\xi_h I_2(\nu_0) = 0.772598 \left(\frac{10^6 M_\odot}{M_h} \right)^{\frac{5}{8}} \left(\frac{2 \text{ keV}}{m} \right)^2 \left(\frac{\Sigma_0 \text{ pc}^2}{120 M_\odot} \right)^{\frac{3}{8}} \quad (2.56)$$

It is illuminating to express the radius r_0 eq.(2.18) in terms of M_{BH} and Σ_0 for large galaxies $M_h \gtrsim 10^6 M_\odot$. It follows from eqs.(2.31), (2.33) and (2.56) that,

$$r_0 = l_0 \xi_0 = 126.762 \sqrt{\frac{10^6 M_\odot}{M_h}} \frac{M_{BH}}{10^6 M_\odot} \sqrt{\frac{120 M_\odot}{\Sigma_0 \text{ pc}^2}} \text{ pc} \quad (2.57)$$

This explicitly provides the value of the radius r_0 in terms of the black hole mass M_{BH} , the halo mass M_h , and the reference surface density Σ_0 .

In summary, we see the power of the WDM Thomas-Fermi approach to describe the structure and the physical state of galaxies in a clear way and in very good agreement with observations.

III. EXPLICIT THOMAS-FERMI GALAXY SOLUTIONS WITH CENTRAL SUPERMASSIVE BLACK HOLES

We solve here the Thomas-Fermi equations (2.13) with the boundary conditions (2.22) for a galaxy with a central black hole.

A. Local thermal equilibrium in the Galaxy

In ref. [13] using the Eddington equation for dark matter in galaxies and observed density profiles, it is shown that the DM halo is realistically a self-gravitating thermal gas for $r \lesssim R_{virial}$. More precisely, the DM halo can be

consistently considered in a local thermal equilibrium situation with: **(i)** a constant temperature T_0 for $r \lesssim 3 r_h$, and **(ii)** a space dependent temperature $T(r)$ for $3 r_h < r \lesssim R_{virial}$, which slowly decreases with r . $T(r)$ outside the halo radius nicely follows the decrease of the circular velocity squared $T_c(r)$ [13]. These results are physically understood because thermalization is more easily achieved in the inner regions due to the fact that the gravitational interaction is stronger than in the external regions where instead virialization occurs. The slow decreasing of the temperature $T(r)$ with the halo radius consistently corresponds to a transfer flux of the kinetic energy into potential energy. These results were derived from empirical observed density profiles which do not have information of the regions near the central black hole.

The constant temperature T_0 for $r \lesssim 3 r_h$ turns to be in the Kelvin scale for a DM particle mass in the keV scale [12].

To implement the Thomas-Fermi approach for a galaxy plus a central black hole we take into account the results of Ref. [13]. We simply set the WDM temperature to be a constant T_0 except in the vicinity of the central black hole. We do not assume WDM thermalization near the central black hole where the black hole force is strong but we assume virialization. Namely, the WDM square velocity is determined by the black hole gravitational field through virialization.

In summary,

- Near the central black hole, the space dependent temperature is given by equipartition and the virial theorem

$$T_c(r) = \frac{m}{3} v_c^2(r) = \frac{G m}{3 r} M_{BH} = \frac{T_0 \xi_0}{3 \xi} \quad (3.1)$$

where we used eqs.(2.9) and (2.18). We use this temperature $T_c(r)$ for $\xi \leq \xi_0/3$. T_0 is given by eq.(2.32).

- For $\xi \geq \xi_0/3$ we set

$$T_c(r) = T_0 .$$

Here the circular temperature $T_c(r)$ associated to the velocity squared is given by

$$T_c(r) = \frac{m}{3} \frac{G [M(r) + M_{BH}]}{r} , \quad (3.2)$$

where $M(r) + M_{BH}$, the mass of the galaxy inside the radius r including the BH mass M_{BH} , is given by eq.(2.40). Inserting eq.(2.40) into eq.(3.2) and using eq.(2.32) yields,

$$T_c(r) = \frac{1}{3} \xi |\nu'(\xi)| T_0 . \quad (3.3)$$

Near the central black hole, that is for $\xi \leq \xi_0/3$, the chemical potential $\nu(\xi)$ is given by eq.(2.18). Inserting eq.(2.18) into eq.(3.3) yields eq.(3.1) as it must be.

- We find from our extensive numerical calculations that the halo is thermalized at the uniform temperature T_0 and matches the circular temperature $T_c(r)$ by $r \sim 3 r_h$. This picture is similar to the picture found in the absence of the central black hole which follows from the observed density profiles in the Eddington-like approach to galaxies [13]. We obtain here in the Thomas-Fermi approach and in the presence of a central supermassive black hole that: the halo is thermalized at a uniform temperature T_0 inside $r \lesssim 3 r_h$ which matches the circular temperature $T_c(r)$ at $r \sim 3 r_h$ [see Fig.4].
- In summary, each galaxy solution with a central black hole depends only on **two free parameters**: the dimensionless constants ξ_0 and A in eq.(2.22). We have a two-parameter family of Thomas-Fermi galaxy solutions with a central supermassive black hole parametrized by ξ_0 and A .

The black hole mass M_{BH} grows when ξ_0 grows as shown by eq.(2.35). Notice that M_{BH} does not simply grow linearly with ξ_0 due to the presence of the factor

$$[\xi_h I_2(\nu_0)]^{-\frac{3}{5}} ,$$

in eq.(2.35).

From our extensive numerical calculations we find that the galaxy mass increases and the galaxy size increases when the constant $|A|$ characteristic of the central behaviour of $\nu(\xi)$ for $\xi \rightarrow 0$ eq.(2.22) increases. This is similar to the case in the absence of central black holes where $A = \nu(0)$ [9], [10], [12].

B. Thomas-Fermi equations with r-dependent temperature $T_c(r)$

For a r -dependent temperature $T_c(r)$ the normalized energy density $I_2(\nu)$ [recall eq.(2.11)] takes the form

$$I_2(\nu) = 3 \int_0^\infty y^2 dy \sqrt{1 + \frac{2y^2}{\tau}} \Psi_{FD} \left(\frac{T_0}{T_c(r)} \left[\tau \left(\sqrt{1 + \frac{2y^2}{\tau}} - 1 \right) - \nu \right] \right) , \quad (3.4)$$

which becomes eq.(2.11) for a constant temperature $T_c(r) = T_0$, that is in the region $\xi \geq \xi_0/3$, ie $r \geq r_0/3$.

Near the BH, for $\xi \leq \xi_0/3$, we have from eq.(3.1),

$$\frac{T_0}{T_c(r)} = \frac{3 \xi}{\xi_0} . \quad (3.5)$$

Beyond $r = 3 r_h$, using eq.(3.3) these quantities take the values

$$\frac{T_0}{T_c(r)} = \frac{3}{\xi |\nu'(\xi)|} \quad (3.6)$$

Notice that $T_c(r)$ grows for $r \rightarrow 0$ as $1/r$ due to the BH presence eq.(3.1). On the contrary, $T_c(r)$ decreases for increasing $r > 3 r_h$.

For a density profile scaling at large r , $r > 3 r_h$, as $r^{-2\alpha}$ we find $T_c(r) \sim r^{2(1-\alpha)}$. Because observations favour $\alpha \sim 1.5 > 1$, $T_c(r)$ decreases for increasing $r > 3 r_h$, as in the case where the black hole is absent [13].

C. Examples of Thomas-Fermi Galaxy solutions with a central supermassive black hole

We consider here three realistic examples: a small mass galaxy, a medium mass and a large mass galaxy. We choose as boundary conditions in eq.(2.22)

$$\begin{aligned} \xi_0 = 1 \quad , \quad A = 0 \quad , \quad \text{small size galaxy} \\ \xi_0 = 7 \quad , \quad A = -10 \quad , \quad \text{medium size galaxy} \\ \xi_0 = 9 \quad , \quad A = -15 \quad , \quad \text{large size galaxy} . \end{aligned} \quad (3.7)$$

These values are illustrative and yield realistic galaxies with a supermassive central black hole as we see below. Indeed, we find realistic solutions for a large manifold of boundary conditions.

To compute these solutions we set as reference values $m = 2$ keV, $\Sigma_0 = 120 M_\odot/\text{pc}^2$.

The present solutions allow to characterize the WDM properties that show up in the different halo regions according to the distance to the central black hole.

For the three representative galaxy solutions eq.(3.7), we plot in Fig. 1 the dimensionless chemical potential $\log_{10} \nu(\xi)$ versus the dimensionless radius $\log_{10}(\xi/\xi_h) = \log_{10}(r/r_h)$, r_h being the halo radius (and ξ_h the dimensionless one) ; in Fig. 2 we plot the derivative $\log_{10} |d\nu(\xi)/dx|$ vs. $\log_{10}(r/r_h)$, and in Fig. 3 we plot the density profiles $\log_{10}[\rho(\xi)/\rho_0]$ vs. $\log_{10}(r/r_h)$, [recall that $\rho_0 \equiv \rho(\xi_i)$, ξ_i being the dimensionless influence radius of the black hole eq.(2.21), that is, when the black hole and dark matter gravitational forces become equal].

Notice that the curves for the three galaxy solutions are of similar size thanks to the use of the rescaled variable $r/r_h = \xi/\xi_h$ in the abscissa. The dimensionless halo radius ξ_h increases by five orders of magnitude going from the small to the large size galaxy.

For the relevant parameters of the solutions we obtain the following results:

Small size galaxy :

$$r_i = 221 \text{ pc} \quad , \quad r_h = 452 \text{ pc} \quad , \quad T_0 = 0.0978 \text{ K},$$

$$\begin{aligned}
\sqrt{\langle v^2 \rangle}(r \gtrsim r_A) &= 35.48 \text{ km/s}, & \sqrt{\langle v^2 \rangle}(r \lesssim r_A) &= 383.75 \text{ km/s}, \\
M_h &= 7.678 \cdot 10^7 M_\odot, & M_{vir} &= 8.582 \cdot 10^8 M_\odot, \\
M_{BH} &= 1.947 \cdot 10^5 M_\odot, & r_{BH}^{Schw} &= 1.863 \cdot 10^{-8} \text{ pc}, \\
\rho_0 &= 1.797 \cdot 10^{-23} \text{ g/cm}^3, \\
\rho_A &= 0.9878 \cdot 10^{-19} \text{ g/cm}^3, & M_A &= 8.767 \cdot 10^4 M_\odot, & r_A &= 1.91 \text{ pc}.
\end{aligned} \tag{3.8}$$

Medium size galaxy :

$$\begin{aligned}
r_i &= 54.3 \text{ pc}, & r_h &= 210 \text{ kpc}, & T_0 &= 26.97 \text{ K}, \\
\sqrt{\langle v^2 \rangle}(r \gtrsim r_A) &= 559.8 \text{ km/s}, & \sqrt{\langle v^2 \rangle}(r \lesssim r_A) &= 6370.9 \text{ km/s}, \\
M_h &= 9.022 \cdot 10^{12} M_\odot, & M_{vir} &= 8.222 \cdot 10^{13} M_\odot, \\
M_{BH} &= 9.224 \cdot 10^7 M_\odot, & r_{BH}^{Schw} &= 8.828 \cdot 10^{-6} \text{ pc}, \\
\rho_0 &= 3.867 \cdot 10^{-26} \text{ g/cm}^3, \\
\rho_A &= 7.182 \cdot 10^{-15} \text{ g/cm}^3, & M_A &= 1.932 \cdot 10^7 M_\odot, & r_A &= 0.2 \text{ pc}.
\end{aligned} \tag{3.9}$$

Large size galaxy :

$$\begin{aligned}
r_i &= 21.66 \text{ pc}, & r_h &= 8.237 \cdot 10^3 \text{ kpc}, & T_0 &= 1061 \text{ K}, \\
\sqrt{\langle v^2 \rangle}(r \gtrsim r_A) &= 3511.2 \text{ km/s}, & \sqrt{\langle v^2 \rangle}(r \lesssim r_A) &= 39591 \text{ km/s}, \\
M_h &= 1.3753 \cdot 10^{16} M_\odot, & M_{vir} &= 3.3482 \cdot 10^{16} M_\odot, \\
M_{BH} &= 1.8632 \cdot 10^9 M_\odot, & r_{BH}^{Schw} &= 1.783 \cdot 10^{-4} \text{ pc}, \\
\rho_0 &= 0.9860 \cdot 10^{-27} \text{ g/cm}^3, \\
\rho_A &= 2.9163 \cdot 10^{-12} \text{ g/cm}^3, & M_A &= 3.873 \cdot 10^8 M_\odot, & r_A &= 0.074 \text{ pc}.
\end{aligned} \tag{3.10}$$

M_A stands for the mass inside the radius r_A .

Notice that the obtained galaxy solutions have halo masses $M_h > 10^6 M_\odot$ and therefore belong to the dilute Boltzmann regime [12].

Let us now analyze the Figures 1-3. We start from the galaxy center and go towards the halo tail.

- **Quantum to classical behaviour:** The central black hole strongly attracts the WDM and makes its density very high for $r < r_A$ where a compact quantum core gets formed. The dimensionless chemical potential $\nu(\xi)$ vanishes at $r = r_A$ and becomes negative for $r > r_A$. The density $\rho(r)$ drops several orders of magnitude immediately after r_A as shown in Fig. 3. $\nu(\xi)$ is negative for $r > r_A$ and the WDM exhibits there a classical Boltzmann behaviour while the WDM exhibits a quantum behaviour for $r < r_A$ where the chemical potential is large and positive. Therefore, the point r_A where the chemical potential vanishes **defines the transition from the quantum to classical behaviour**. In the quantum region $r < r_A$ the density exhibits a constant plateau as shown in Fig. 3. Notice from eqs.(3.8) that r_A turns to be much larger than the Schwarzschild radius of the central black hole $r_A \gg r_{BH}^{Schw}$.
- **Black hole influence radius r_i :** For $r < r_i$ the black hole gravitational field dominates over the dark matter gravitational field. The influence radius $r_i = l_0 \xi_i$ is defined by eq.(2.21). The black hole influence radius turns to be larger than the radius r_A where the chemical potential vanishes, $r_i > r_A$. The region $r_A < r < r_i$ is

dominated by the central black hole and the WDM exhibits there a classical behaviour. For $r \lesssim r_i$, we see from Figs. 1-2 that both $\nu(\xi)$ and $|d\nu(\xi)/dx|$ follow the behaviour dictated by the central black hole. That is, from eq.(2.22)

$$\nu(\xi) \simeq \xi_0 e^{-x} + A = \xi_0 \frac{r_h}{r} + A \quad , \quad |d\nu(\xi)/dx| \simeq \xi_0 e^{-x} = \xi_0 \frac{r_h}{r} \quad , \quad x \equiv \ln \frac{r}{r_h} \quad ,$$

which produce straight lines on the left part of the logarithmic plots Figs. 1-2. For $r \gtrsim r_i$, $\nu(\xi)$ and $|d\nu(\xi)/dx|$ are dominated by the WDM and exhibit a similar behaviour to that of the Thomas-Fermi solutions without a central black hole [9], [10], [11], [12].

Fig. 3 shows that the local density behaviour is dominated by the black hole for $r \lesssim r_i$. Coherently, for $r \gtrsim r_i$ the WDM gravitational field dominates over the black hole field and the galaxy core shows up for $r_i \lesssim r \lesssim r_h$ in Fig. 3. For medium and large galaxies the core is seen as a plateau. At the same time the chemical potential is negative for $r \gtrsim r_i > r_A$ and the WDM is a classical Boltzmann gas in this region.

- **Halo radius r_h :** Finally, we see in Fig. 3 the tail of the WDM density profile for $r \gtrsim r_h$ which exhibit a similar shape for all three galaxy solutions.
- **WDM thermalization:** As shown by Fig. 4, the velocity dispersion $\langle v^2 \rangle (r)$ is constant as a function of r indicating a thermalized WDM with temperature

$$T_0 = \frac{1}{3} m \langle v^2 \rangle \quad .$$

WDM gets thermalized as in the absence of the central black hole [12]. This is consistent with the use of a thermal Fermi-Dirac distribution function for $r \geq r_0/3$.

- We also plot in Fig. 4 the circular velocity given by eq.(2.48) vs. $\log_{10} r/r_h$. For $r > r_h$ the circular velocity tends to the velocity dispersion as obtained from the Eddington equation for realistic density profiles [13]. For $r \rightarrow 0$ the circular velocity grows as in eq.(2.49) due to the central black hole field.
- WDM inside a small core of radius r_A is in a quantum gas high density state, namely a Fermi nearly degenerate state with nearly constant density ρ_A . For the three galaxy solutions, the values of r_A and ρ_A are given by eqs.(3.8)-(3.10). Notice, that the density ρ_A is orders of magnitude larger than its values for $r > r_A$ where the WDM is in the classical Boltzmann regime.
- We also give in eqs.(3.8)-(3.10) the WDM mass M_A inside r_A . M_A represents only a small fraction of the halo or virial mass of the galaxy but it is a significant fraction of the black hole mass M_{BH} . We see from eqs.(3.8)-(3.10) that M_A amounts for 20% of M_{BH} for the medium and large galaxies and 45% for the small galaxy.

D. Quantum physics in galaxies

In order to determine whether a physical system has a classical or quantum nature one has to compare the average distance between particles d with their de Broglie wavelength λ_{dB} .

The de Broglie wavelength of DM particles in a galaxy can be expressed as

$$\lambda_{dB}(r) = \frac{h}{m v(r)} \quad , \quad (3.11)$$

where h stands for the Planck constant and $v \equiv \sqrt{\langle v^2 \rangle}$ is the velocity dispersion, while the average interparticle distance d at r can be estimated as

$$d(r) = \left(\frac{m}{\rho(r)} \right)^{\frac{1}{3}} \quad (3.12)$$

Here $\rho(r)$ is the local density in the galaxy core.

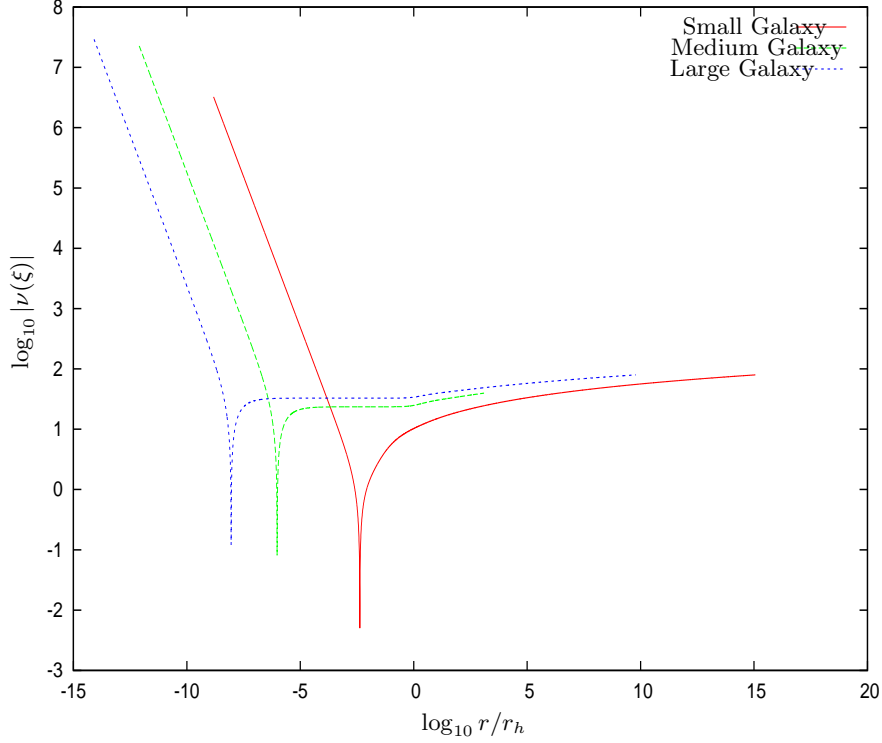


FIG. 1: The dimensionless chemical potential $\log_{10} |\nu(\xi)|$ vs. $\log_{10}(\xi/\xi_h) = \log_{10}(r/r_h)$ for the three illustrative galaxy solutions with central SMBH defined by eq.(3.7). $\nu(\xi)$ is negative for $r > r_A = l_0 \xi_A$ and WDM exhibits there a classical dilute Boltzmann gas behaviour, while WDM exhibits a compact quantum gas behaviour for $r < r_A$ where the chemical potential is positive. The point r_A where the chemical potential vanishes **defines the transition from the quantum to the classical galaxy WDM behaviour**. r_A is at the downward spike of $\log_{10} |\nu(\xi)|$ where $\nu(\xi)$ vanishes.

We can measure the classical or quantum character of the system by considering the ratio

$$\mathcal{R}(r) \equiv \frac{\lambda_{dB}(r)}{d(r)}$$

For $\mathcal{R} \lesssim 1$ the system is of classical dilute nature while for $\mathcal{R} \gtrsim 1$ it is a macroscopic quantum system.

By using the phase-space density eq.(2.45),

$$Q(r) = \frac{\rho(r)}{\sigma^3(r)},$$

and eqs.(3.11)-(3.12), $\mathcal{R}(r)$ can be expressed solely in terms of the phase space-density $Q(r)$ as [9], [10],[12]

$$\mathcal{R}(r) = \frac{2\pi}{\sqrt{3}} \hbar \left(\frac{Q(r)}{m^4} \right)^{\frac{1}{3}}. \quad (3.13)$$

Inserting the phase-space density eq.(2.45) into eq.(3.13) yields for the ratio $\mathcal{R}(r)$,

$$\mathcal{R}(r) = 2\sqrt{5} \left(\frac{\pi}{81} \right)^{\frac{1}{3}} \frac{I_2^{\frac{5}{6}}(\nu(\xi))}{I_4^{\frac{1}{2}}(\nu(\xi))} = 1.513805 \frac{I_2^{\frac{5}{6}}(\nu(\xi))}{I_4^{\frac{1}{2}}(\nu(\xi))}. \quad (3.14)$$

In Fig. 5 we plot $\log_{10} \mathcal{R}$ vs. $\log_{10}(r/r_h)$ for the three representative galaxy solutions.

Comparing now Figs.1 and 5 we see that $\nu(\xi)$ **changes sign** indicating the transition from the quantum to the classical galaxy regime **precisely at the same point** where $\mathcal{R} \simeq 1$, as it must be. This result shows the power and consistency of our treatment.

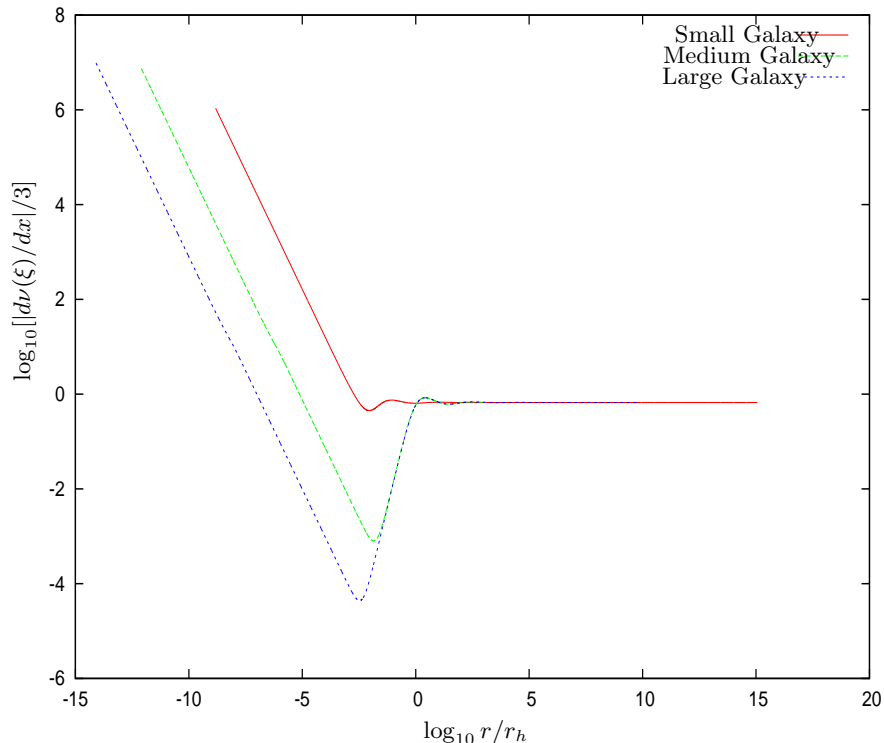


FIG. 2: The derivative of the dimensionless chemical potential $\log_{10}[|d\nu(\xi)/dx|/3]$ vs. $\log_{10}(\xi/\xi_h) = \log_{10}(r/r_h)$ for the three galaxy solutions with central SMBHs defined by eq.(3.7). For $r \lesssim r_i$ both $\nu(\xi)$ and $|d\nu(\xi)/dx|$ follow the behaviour dictated by the central black hole. r_i is the influence radius of the BH defined by eq. (2.21). For $r \gtrsim r_i$, $\nu(\xi)$ and $|d\nu(\xi)/dx|$ are dominated by WDM and exhibit a similar behaviour to that for the Thomas-Fermi galaxy solutions without a central black hole [9–12].

IV. SYSTEMATIC STUDY OF THE THOMAS-FERMI GALAXY SOLUTIONS WITH A CENTRAL SUPERMASSIVE BLACK HOLE

We present in this section our extensive study of the Thomas-Fermi Galaxy solutions with a central supermassive black hole.

As stated in subsection III A, each galaxy solution with a central black hole depends only on **two free parameters**: ξ_0 and A defining the boundary conditions near the center [see eq.(2.22)], ξ_0 being the dimensionless central radius and A characterizing the central chemical potential behaviour.

We plot in Fig. 6 the halo mass $\log_{10} M_h$ vs. A for fixed values of ξ_0 .

We see that the halo mass M_h increases with ξ_0 at fixed A . In addition, at fixed $\xi_0 > 0$, M_h increases when the absolute value of A increases .

There is an **important qualitative** difference between galaxy solutions with a black hole ($\xi_0 > 0$), and galaxy solutions without a black hole ($\xi_0 = 0$). In the absence of the central black hole, the halo mass M_h monotonically decreases when A increases till M_h reaches a minimal value which is the degenerate quantum limit at zero temperature [9], [10], [12]:

$$M_h^{min} = 3.0999 \cdot 10^4 \left(\frac{2 \text{ keV}}{m} \right)^{\frac{16}{5}} \left(\frac{\Sigma_0 \text{ pc}^2}{120 M_\odot} \right)^{\frac{3}{5}} M_\odot, \quad T_0^{min} = 0, \quad \text{without central black hole} . \quad (4.1)$$

In the presence of a central black hole, we find that the halo mass takes as minimal value

$$M_h^{min} = 6.892 \cdot 10^7 \left(\frac{2 \text{ keV}}{m} \right)^{\frac{16}{5}} \left(\frac{\Sigma_0 \text{ pc}^2}{120 M_\odot} \right)^{\frac{3}{5}} M_\odot, \quad \text{with central black hole} . \quad (4.2)$$

This situation is clearly shown in Fig. 6. The value of M_h^{min} with a central black hole is $2.2233 \cdot 10^3$ times larger

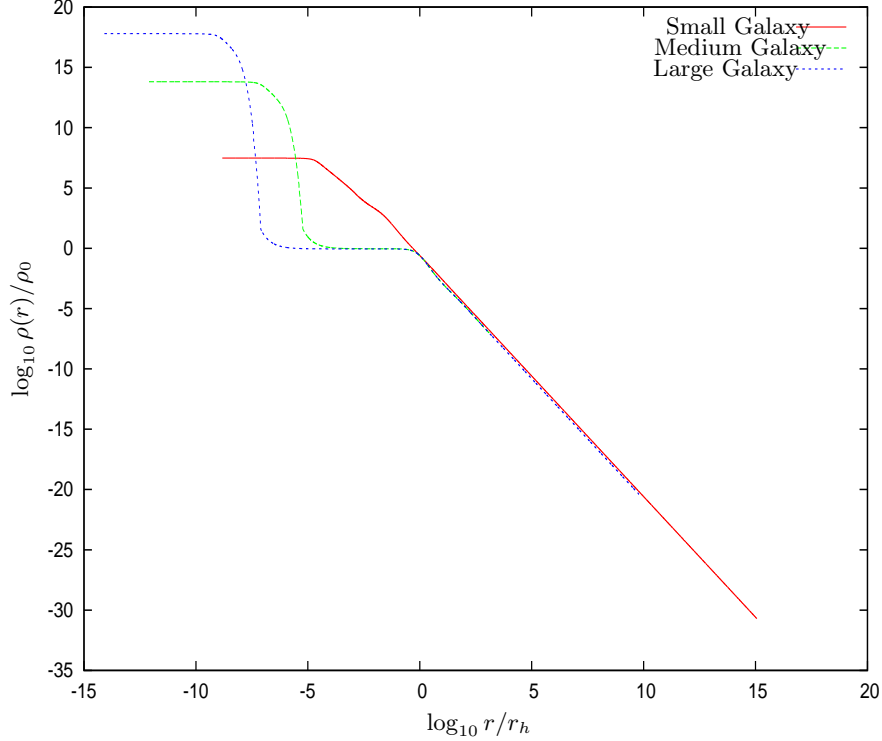


FIG. 3: The density ρ normalized at the influence radius r_i , $\log_{10}(\rho(r)/\rho_0)$ vs. $\log_{10}(r/r_h)$ for the three galaxy solutions with central SMBHs. Notice that in the quantum gas WDM region $r < r_A$ the density is constant clearly exhibiting a plateau behaviour corresponding to the quantum Fermi gas behaviour in such region.

than without the black hole. Notice that the small galaxy solution eq.(3.8) is just 11 % larger in halo mass than the minimal galaxy eq.(4.2) with central black hole.

We conclude that galaxies possessing a central black hole are in the dilute Boltzmann regime because of their large mass $M_h > M_h^{min}$ [12]. In addition, compact galaxies with $M_h < M_h^{min}$, in particular ultracompact galaxies in the quantum regime $M_h < 2.3 \cdot 10^6 M_\odot$ [12], **cannot** harbor central black holes.

We plot in Fig. 7 the galaxy temperature $\log_{10} T_0/\text{K}$ vs. the characteristic central chemical potential constant A for fixed values of ξ_0 .

Similarly to the halo mass M_h , the galaxy temperature T_0 increases with ξ_0 at fixed A . On the other hand, at fixed $\xi_0 > 0$, T_0 increases when the absolute value of A increases.

In the absence of a black hole, the galaxy temperature T_0 tends to zero for $A \rightarrow \infty$, while in the presence of a central black hole we find that T_0 is always *larger* than the *non zero minimal value*:

$$T_0^{min} = 0.06928 \left(\frac{2 \text{ keV}}{m} \right)^{\frac{3}{5}} \left(\frac{\Sigma_0 \text{ pc}^2}{120 M_\odot} \right)^{\frac{4}{5}} \text{ K}, \quad \text{with central black hole.} \quad (4.3)$$

The presence of the supermassive black hole **heats-up** the dark matter gas and prevents it to become an exact degenerate gas at zero temperature. The minimal mass and size and most compact galaxy state with a supermassive black hole is a nearly degenerate state at very low temperature as seen from eq. (4.3).

The mass of the supermassive black hole M_{BH} monotonically increases with ξ_0 at fixed A . In addition, for $\xi_0 < 0.3$, that is for small supermassive black holes, and all A , the galaxy parameters as halo mass M_h , halo radius r_h , virial mass M_{vir} and galaxy temperature T_0 become **independent** of ξ_0 showing a *limiting galaxy solution*. Only the BH mass depends on ξ_0 in this regime.

We depict in Fig. 8 the black hole mass $\log_{10} M_{BH}$ vs. the halo mass $\log_{10} M_h$. We see that M_{BH} is a **two-valued** function of M_h . For each value of M_h there are two possible values for M_{BH} . These two values of M_{BH} for a given M_h are quite close to each other. This two-valued dependence on M_h is a direct consequence of the dependence of M_h on A shown in Fig. 6.

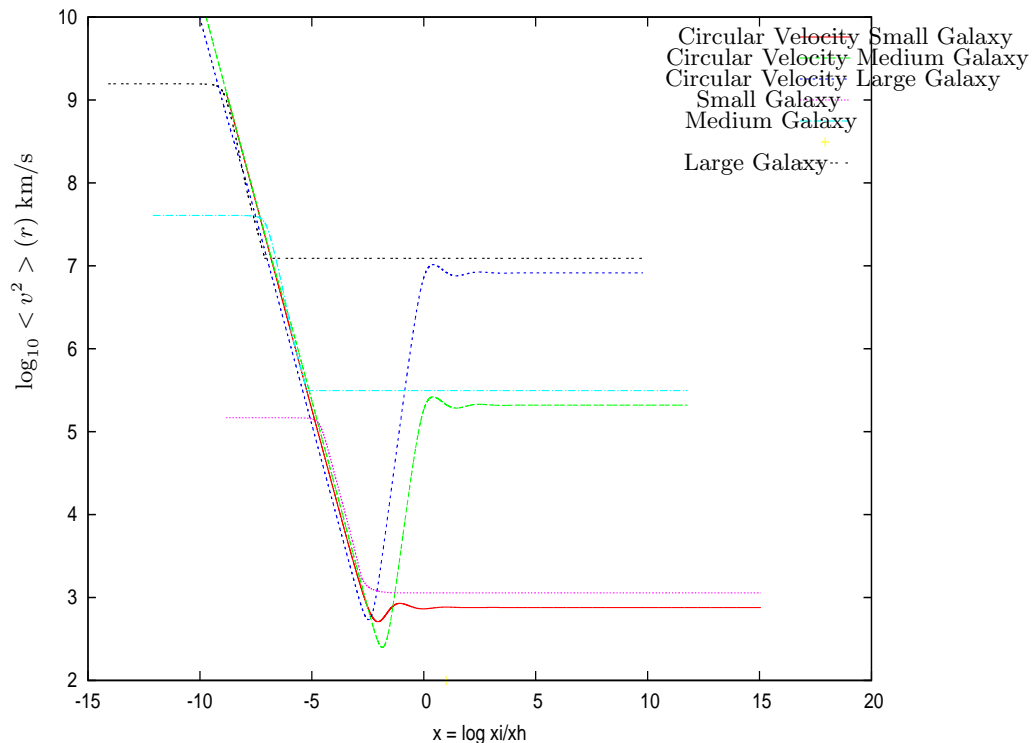


FIG. 4: The velocity dispersion $\langle v^2 \rangle(r)$ and the circular velocity $v_c^2(r)$ for the three representative galaxy solutions with central SMBH vs. $\log_{10}(r/r_h)$. The velocity dispersion is constant in the Boltzmann and in the quantum regions indicating a thermalized WDM with two different temperatures $T_0 = \frac{1}{3} m \langle v^2 \rangle(r)$. For $r > r_h$ the circular velocity tends to the velocity dispersion [13]. These results are in agreement with the DM thermalization found in the absence of a central BH [13], [12].

We see at the branch-points on the left in Fig. 8, the minimal galactic halo mass M_h^{min} eq.(4.2) when a supermassive black hole is present.

At **fixed** ξ_0 , as shown in Fig. 8, the central black hole mass M_{BH} scales with the halo mass M_h as

$$M_{BH} = D(\xi_0) M_h^{\frac{3}{8}},$$

where $D(\xi_0)$ is an increasing function of ξ_0 .

- We plot in Fig. 9 the halo galaxy mass $\log_{10} M_h$ vs. the galaxy temperature $\log_{10} T_0/K$. The halo mass M_h grows when T_0 increases. Colder galaxies are smaller. Warmer galaxies are larger.

We see at the branch-points in Fig. 9 the minimal galaxy temperature T_0^{min} eq.(4.3) when a supermassive black hole is present.

- We find galaxy solutions with central black holes for arbitrarily small values $\xi_0 > 0$ and correspondingly arbitrarily small central BH mass. There is no emergence of a minimal mass for the central black hole.

A. Universal Scaling relations in the presence of central black holes

We plot in Fig. 10 the ordinary logarithm of the halo radius $\log_{10} r_h$ vs. the ordinary logarithm of the halo mass $\log_{10} M_h$ for galaxies with central black holes of many different masses. We see in **all cases** that M_h scales as r_h^2 . The same scaling was found in the Thomas-Fermi approach to galaxies in absence of black holes [9], [10], [12].

The halo mass in the absence of a central black hole behaves in the Thomas-Fermi approach as [12]

$$M_h = 1.75572 \Sigma_0 r_h^2, \quad \text{without central black hole.} \quad (4.4)$$

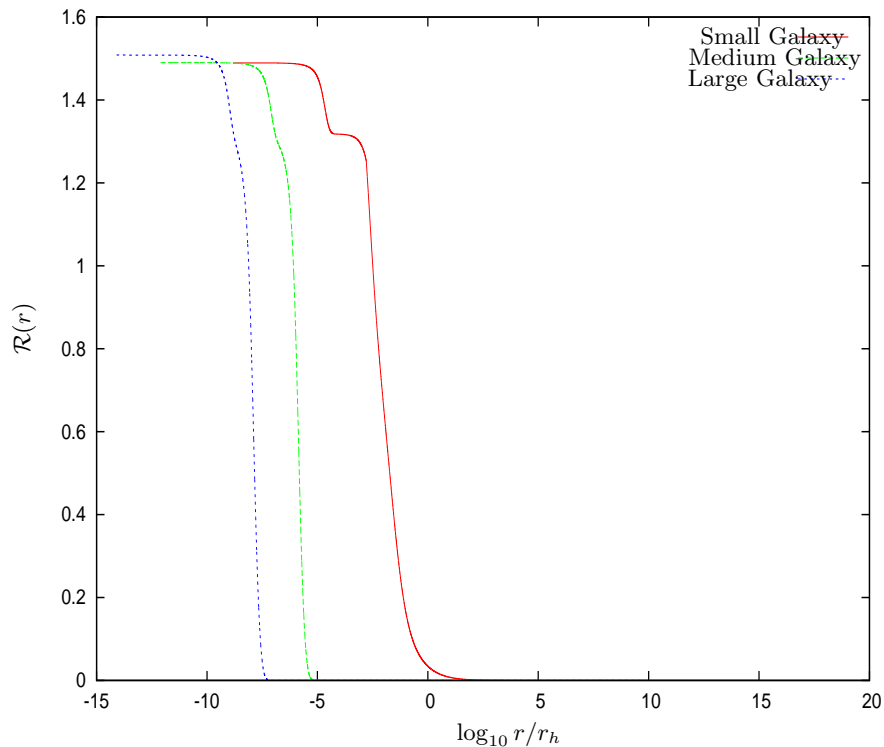


FIG. 5: The ratio \mathcal{R} of the particle de Broglie wavelength to the interparticle distance in the galaxy as a function of r for the three representative galaxy solutions with central SMBH: Small galaxy (red), Medium galaxy (green), Large galaxy (blue). For $\mathcal{R} \lesssim 1$ the galaxy plus SMBH system is of classical nature while for $\mathcal{R} \gtrsim 1$ the system is quantum. The transition from the quantum to the classical regime occurs precisely at **the same point** r_A where the chemical potential vanishes (see Fig. 1) showing the consistency and power of our treatment. This point defines the transition from the quantum to the classical behaviour.

The proportionality factor in this scaling relation is confirmed by the galaxy data [12].

In the presence of a central black hole we find in the Thomas-Fermi approach an analogous relation

$$M_h = b \Sigma_0 r_h^2 \quad , \quad \text{with central black hole} \quad , \quad (4.5)$$

where the coefficient b turns to be of order unity.

We plot in Fig. 11 the coefficient b as a function of the halo mass M_h . We see that except for halo masses near the minimum halo mass M_h^{min} , b in the presence of a central black hole takes values up to 10% below its value in the absence of a central black hole eq.(4.4). For halo masses near M_h^{min} , b increases reaching values $b \leq 4$. For very large halos and central black holes, b could be as small as about 1.6.

That is, the coefficient b changes at most by a factor from 1/2 up to 2 while the halo mass M_h varies ten orders of magnitude. As shown by Fig.11, the coefficient b turns to be a two-valued function of M_h .

The coefficient b turns to be independent of the precise value of the WDM particle mass m . This is due to the fact that the scaling relation eq.(4.5) as well as eq.(4.4) apply in the classical Boltzmann regime of the galaxy.

In summary, the scaling relation eq.(4.5) and the coefficient b turn out to be remarkably robust.

We plot in Fig. 12 the ordinary logarithm of the halo radius $\log_{10} r_h$ versus the ordinary logarithm of the central black hole mass $\log_{10} M_{BH}$ for many galaxy solutions. The halo radius r_h turns to be a double-valued function of M_{BH} . **Remarkably**, r_h scales for **fixed** ξ_0 as

$$r_h = C(\xi_0) M_{BH}^{\frac{4}{3}}. \quad (4.6)$$

The constant $C(\xi_0)$ turns out to be a decreasing function of ξ_0 .

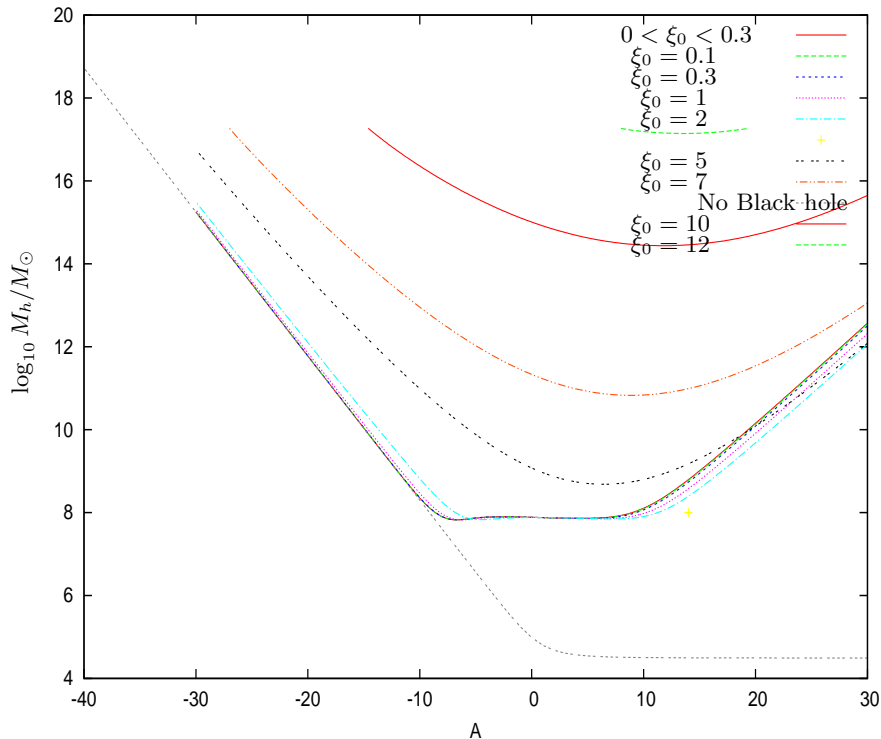


FIG. 6: The halo mass $\log_{10} M_h$ vs. the constant A of the chemical potential behaviour at the origin for fixed values of ξ_0 . The halo mass M_h increases with ξ_0 at fixed A . M_h increases when the absolute value of A increases at fixed $\xi_0 > 0$. In absence of the central black hole, the halo mass monotonically decreases when A increases till M_h reaches its *minimal value* eq.(4.1) at the degenerate quantum limit *at zero temperature* [9, 10, 12]. In the presence of a central black hole, we find a *larger* minimal value for the halo mass M_h^{min} eq.(4.2) with a *non zero minimal temperature* T_0^{min} eq.(4.3). Therefore, there is an **important qualitative** difference between galaxy solutions with a black hole $\xi_0 > 0$, and galaxy solutions without a black hole $\xi_0 = 0$.

B. Pressure and equation of state in the presence of central black holes

The local pressure $P(r)$ is given by eq. (2.43). In Fig. 13 we plot $\log_{10} P(r)$ vs. $\log_{10}(r/r_h)$ for the three representative galaxy solutions. We see that $P(r)$ monotonically decreases with r . The pressure $P(r)$ takes huge values in the quantum (high density) region $r < r_A$ and then it sharply decreases entering the classical (dilute) region $r > r_A$.

In Fig. 14 we plot $\log_{10} P(r)$ vs. $\log_{10} \rho(r)/\rho_0$ for the three galaxy solutions with central SMBH. We see that the three curves almost coincide and that they are almost straight lines of unit slope. That is, the equation of state is in very good approximation a perfect gas equation of state. This perfect gas equation of state stems from the fact that galaxies with central black holes have halo masses $M_h > M_h^{min}$ eq.(4.2) and therefore belong to the *dilute* Boltzmann classical regime [12]. The equation of state turns out a local (r -dependent) perfect gas equation of state because of the gravitational interaction, (WDM self-gravitating perfect gas).

Indeed, for galaxies with central black holes the WDM is in a quantum (highly compact) regime inside the quantum radius r_A . However, because r_A is in the parsec scale or smaller [see eqs.(3.8)-(3.10)] the bulk of the WDM is in the Boltzmann classical regime which consistently reflects in the perfect gas equation of state behaviour.

V. CONCLUSIONS

- We have presented here a novel study of galaxies with central supermassive black holes which shows itself fruitful and enlightening. This framework stress the key role of gravity and warm dark matter in structuring galaxies with their central supermassive black holes and provides correctly the major physical quantities to be first obtained for the galaxy-black hole system: the masses, sizes, densities, velocity dispersions, and their internal physical states. This also yields a physical and precise characterisation of whether they are compact,

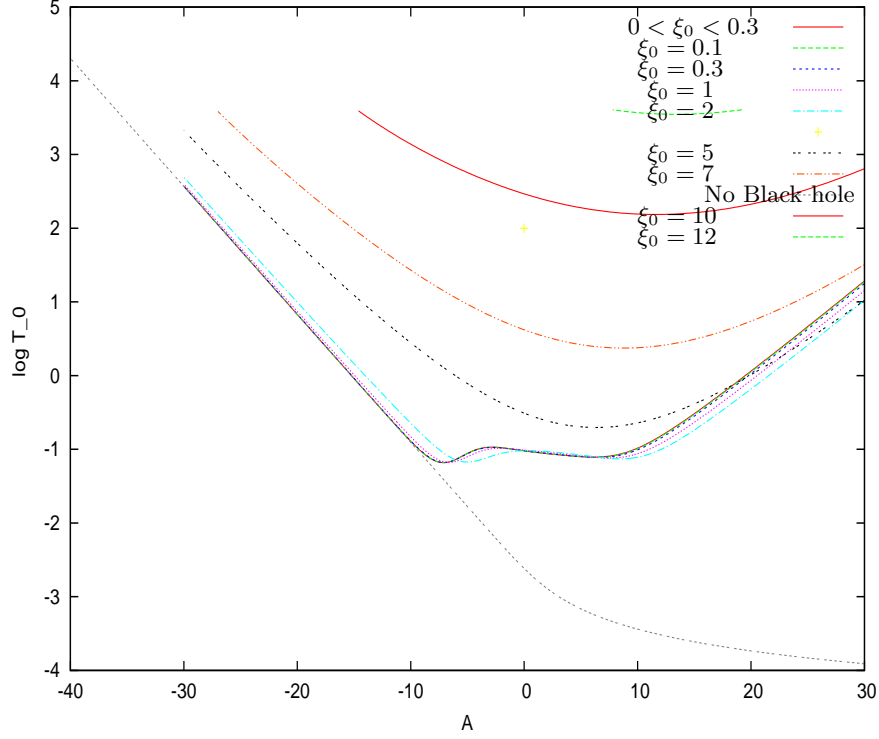


FIG. 7: The galaxy temperature $\log_{10}(T_0/\text{K})$ vs. the constant A of the chemical potential behaviour at the origin, for fixed values of ξ_0 . As for the halo mass M_h , the galaxy temperature T_0 increases with ξ_0 at fixed A . T_0 increases when the absolute value of A increases at fixed $\xi_0 > 0$. In the absence of a black hole, the galaxy temperature T_0 tends to zero for $A \rightarrow \infty$ (at the exact Fermi degenerate state) while in the presence of a central black hole, we find that T_0 is always larger than a minimal non-zero value T_0^{min} given by eq.(4.3).

ultracompact, low density or large dilute galaxies, encompassed with their classical physics and quantum gas physical properties.

- We thus found different regions structuring internally the halo of the galaxy from the vicinity of the supermassive central black hole region to the external regions or virial radius. For all galaxy arboring a central black hole there is a transition from the quantum to the classical regime going from the more compact inner regions which are in a quantum gas state till the classical dilute regions in a Boltzmann-like state. This is accompanied by a decreasing of the local temperature from the central warmer regions to the colder external ones. The SMBH heats the DM near around and prevents it to become exactly degenerated at zero temperature. Although the inner DM quantum core is highly compact in a nearly degenerate quantum gas state, it is not at zero temperature. Inside $r \lesssim 3 r_h$ the halo is thermalized at a uniform or slowly varying local temperature T_0 which tends to the circular temperature $T_c(r)$ at $r \sim 3 r_h$.
- We have formulated the problem of galaxy structure with central supermassive black holes in the WDM Thomas-Fermi approach and found the main physical magnitudes and properties of the galaxy plus black hole system. We solved the corresponding equations and boundary conditions, find three representative families of realistic galaxy solutions (small, medium and large size galaxies) with central supermassive black holes and provided a systematic analysis of the new quantum and classical physics properties of the system. The approach naturally incorporates the quantum pressure of the self-gravitating dark matter fermions showing its full power and clearness to treat the galaxy plus supermassive black hole system. The realistic astrophysical masses of supermassive black holes are naturally obtained in this framework.
- We found the main important physical differences between galaxies with and without the presence of a central black hole. In the presence of a central black hole, both the quantum and classical behaviours of the dark matter gas do co-exist generically in any galaxy from the compact small galaxies to the dilute large ones and a novel galaxy halo structure with three regions show up.
- The transition from the quantum to classical regime occurs at the point r_A where the chemical potential vanishes

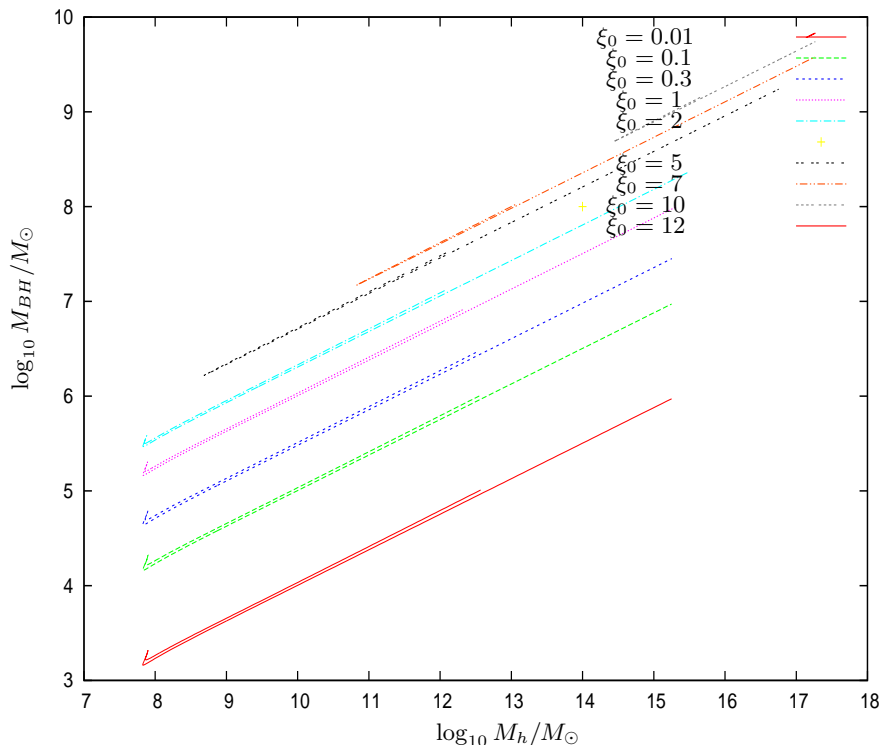


FIG. 8: The black hole mass $\log_{10} M_{BH}$ vs. the halo mass $\log_{10} M_h$. The black hole mass M_{BH} turns out to be a **two-valued** function of M_h . For each value of M_h there are two values for M_{BH} . These two values of M_{BH} for a given M_h are quite close to each other. This two-valued dependence on M_h is a direct consequence of the dependence of M_h on the central chemical potential behaviour characterized by the constant A as shown in Fig. 6.

and which is in addition, precisely and consistently, the point where the particle wavelength and the interparticle distance are equal (their ratio being a measure of the quantum or classical properties of the system). The quantum radius r_A is larger for the smaller and more compact galaxies and diminishes with increasing galaxy and black hole masses for the large dilute galaxies. The WDM mass M_A inside the quantum galaxy radius r_A represents only a small fraction of the halo mass M_h or virial mass of the galaxy but it is a significant fraction of the black hole mass M_{BH} . M_A amounts for 20% of M_{BH} for the medium and large galaxies and 45% for the small galaxies.

- The minimal mass M_h^{min} a galaxy should have in order to harbor SMBHs have been found, which shows among other features why compact or ultracompact galaxies (in the range $10^4 M_\odot < M_h < 10^7 M_\odot$) cannot harbor necessarily central black holes.
- Novel universal scaling relations in the presence of a central supermassive black hole have been derived: black hole mass M_{BH} - halo radius r_h - halo mass M_h relations. The black hole mass M_{BH} turns out to be a two-valued function of the halo mass M_h and size r_h , and we found the local pressure and equation of state of the galaxy-black hole system and its different regimes.
- A more detailed quantitative account of the main features and results of this paper is presented in the Introduction-Section I.
- The circular velocities, galactic rotation curves in the WDM halo with central SMBH are discussed, self-consistently computed and plotted in Section II, Eqs (2.46) to (2.49), Eqs (2.53)-(2.54) and Fig.4 of this paper together with the obtained velocity dispersions. These results are presented for the three family of galaxy solutions with SMBHs obtained here with this approach: Small or Dwarf Galaxies, Medium Galaxies and Large Galaxies. They remarkably encompass the other relevant physical magnitudes obtained for these systems in this paper with the same approach. Towards the central regions, the circular velocity grows as in eq.(2.49) due to the central black hole field. As seen from Fig 4, the dispersion velocity is constant in the Boltzmann (outer or classical) region and in the quantum (inner or compact) region, indicating WDM thermalization. For $r > r_h$, the circular velocity tends to the velocity dispersion. Remarkably, this result confirms the same behaviour we

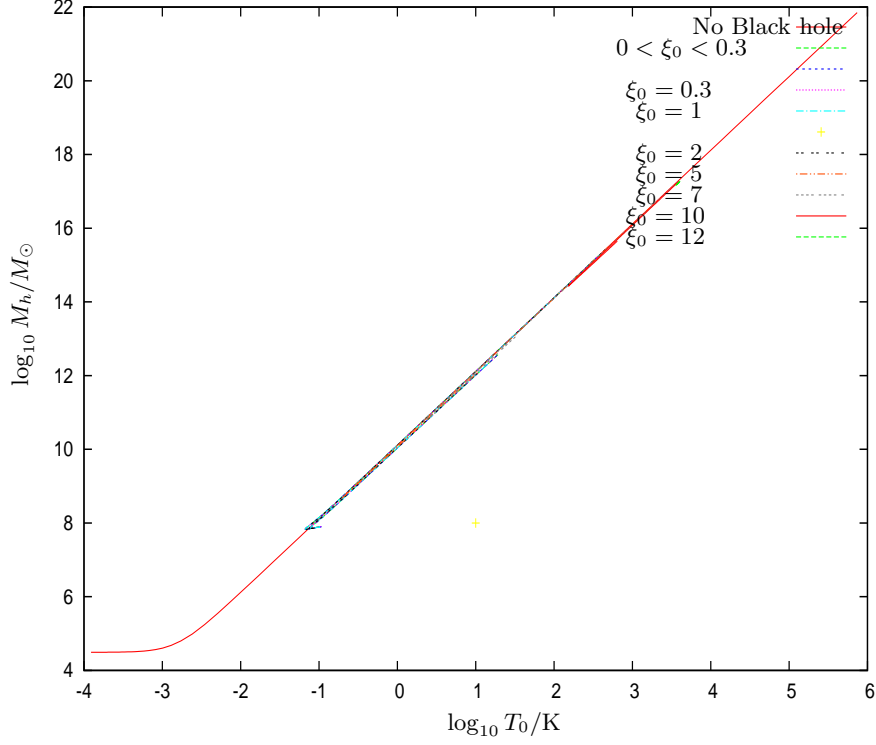


FIG. 9: The halo galaxy mass $\log_{10} M_h$ vs. the galaxy temperature $\log_{10} T_0/K$. M_h turns to be a **two-valued** function of T_0 . The halo mass M_h grows when T_0 increases. Colder galaxies are smaller while warmer galaxies are larger. We see at the branch-points in Fig. 9 the minimal galaxy temperature T_0^{min} eq.(4.3) when a supermassive black hole is present.

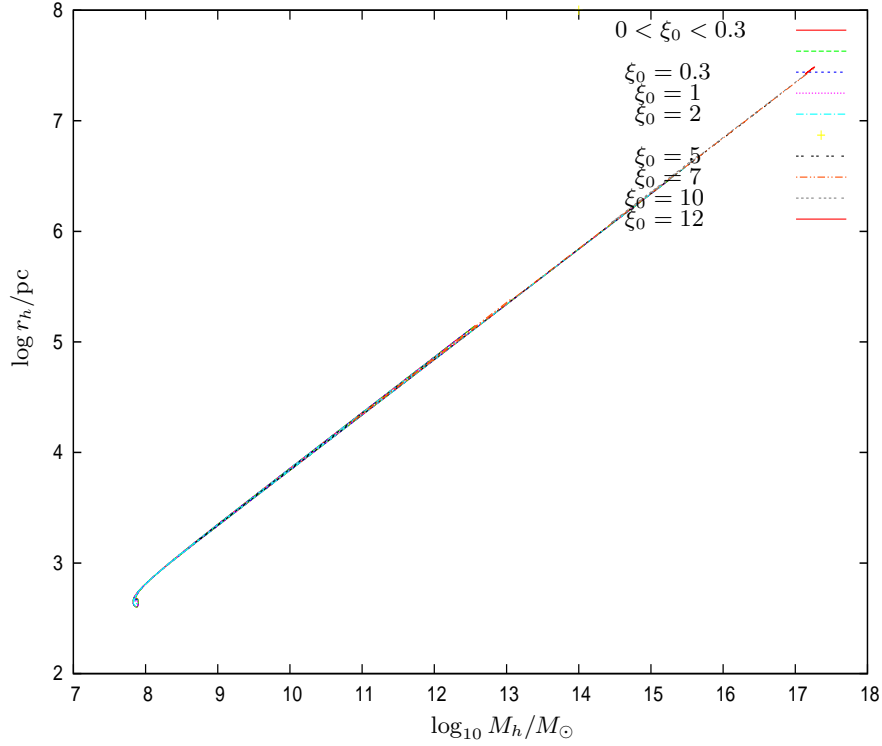


FIG. 10: The halo radius $\log_{10} r_h$ vs. the common logarithm of the halo mass $\log_{10} M_h$ for galaxies with supermassive central black holes of many different masses. r_h turns to be a **two-valued** function of M_h . We see that M_h accurately scales as r_h^2 . The same scaling was found in the Thomas-Fermi approach for galaxies in the absence of black holes [9, 10, 12].

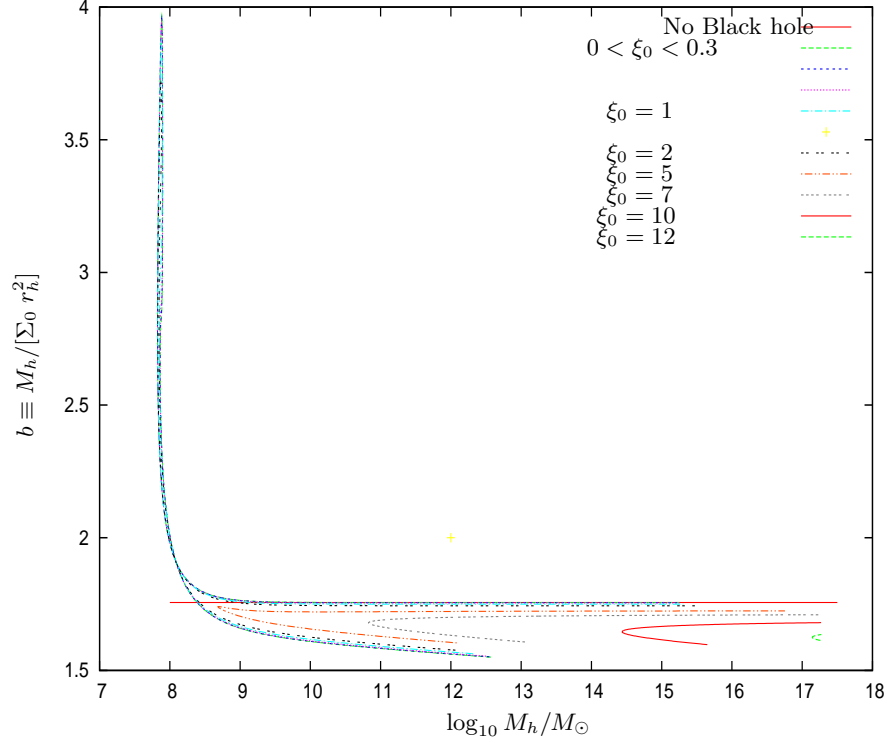


FIG. 11: The scaling amplitude $b \equiv M_h / [\Sigma_0 r_h^2]$ as a function of the halo mass M_h . Except for halo masses near the minimum halo mass M_h^{min} eq.(4.2), b in the presence of a central black hole takes values up to 10% below its value 1.75572 in the absence of a central black hole eq.(4.4). The continuous red horizontal line $b = 1.75572$ corresponds to galaxies without central black holes [eq.(4.4)].

obtained independently with a different approach (the inverse problem or the Eddington integral equation for galaxies which we developed in Ref [13]), namely : given the observed density profiles as input, the velocities, pressure and other galaxy magnitudes are obtained and analyzed as output. The observed density profiles being by definition real realistic data, the obtained results from them are trustable realistic magnitudes. Moreover, another robust verification of the keV WDM Thomas-Fermi approach are the 10 independent sets of observational data we used in Ref [11] for galaxy masses from $5 \cdot 10^9 M_\odot$ to $5 \cdot 10^{11} M_\odot$. The theoretical and observational rotation curves do agree. In addition, they agree extremely well with the observational rotation curves described by the empirical Burkert profile for $r \geq 2r_h$. (they differ from each other by only 2.4 per cent). These results show the success of the keV WDM Thomas-Fermi approach to correctly describe the galaxy structures.

- We have first investigated pure WDM galaxies with their central black holes, because DM is on average the over-dominant component in galaxies, and it is reasonable then to investigate first the effects of gravity plus WDM. This is thus a first approximation, more precisely the zero order of a first approximation in which the visible matter component, baryons, can be incorporated to provide a most accurate and complete picture. We have seen, that these zero order results found here are already realist very good and robust results and they set the basis and the direction for improvements and a more complete understanding.
- Baryons will provide corrections to this picture and will allow to study other processes in which ordinary matter naturally plays a role as the gas and star components, but baryons will not change drastically the pure WDM results found here which are the structural galaxy and black hole properties, masses, sizes, their scaling and relations, density profiles, the classical and quantum nature of the halo regions and their physical, high density, medium density or dilute state, the halo thermalization and virialization.
- This predictive theory and the obtained classes of solutions include very well the different galaxy types through their generic and important physical quantitative properties as the pressure, density, equation of state, mass, halo structure, central black holes. Thus, we have primarily three galaxy classes: large dilute galaxies, intermediate galaxies, and small compact galaxies, whatever their astronomical empirical/historical name. The *Milky Way* galaxy is one of the galaxies in the large dilute galaxy class we found with all the specific properties of this

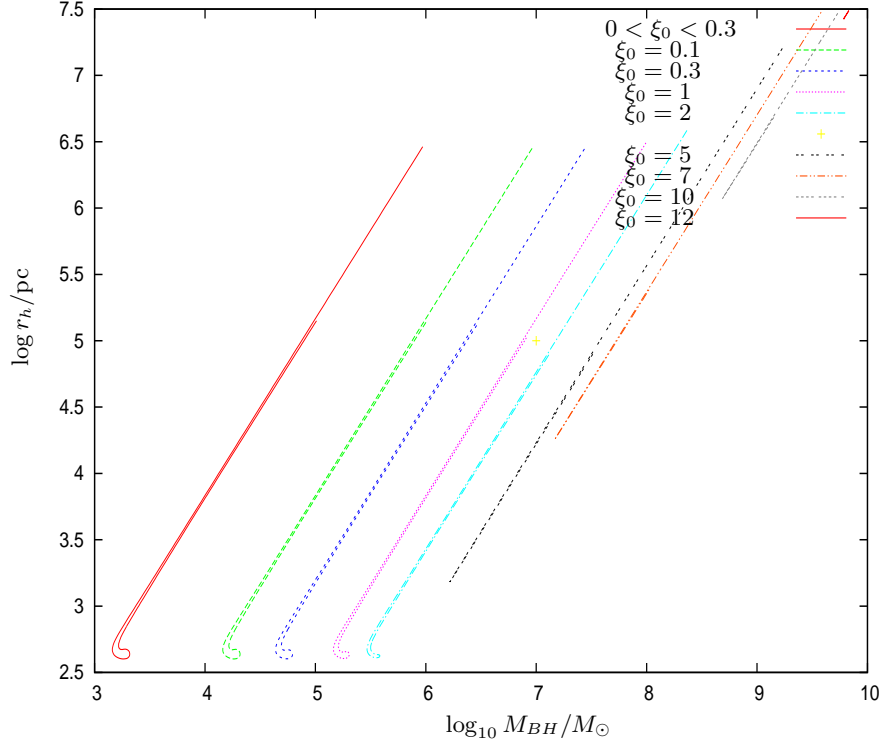


FIG. 12: The common logarithm of the halo radius $\log_{10} r_h$ vs. the common logarithm of the central black hole mass $\log_{10} M_{BH}$ for many galaxy solutions. The halo radius r_h turns to be a **double-valued function** of M_{BH} . Remarkably, r_h scales with the black hole mass for fixed ξ_0 as $r_h = C(\xi_0) M_{BH}^{\frac{4}{3}}$ where the constant $C(\xi_0)$ is a decreasing function of ξ_0 .

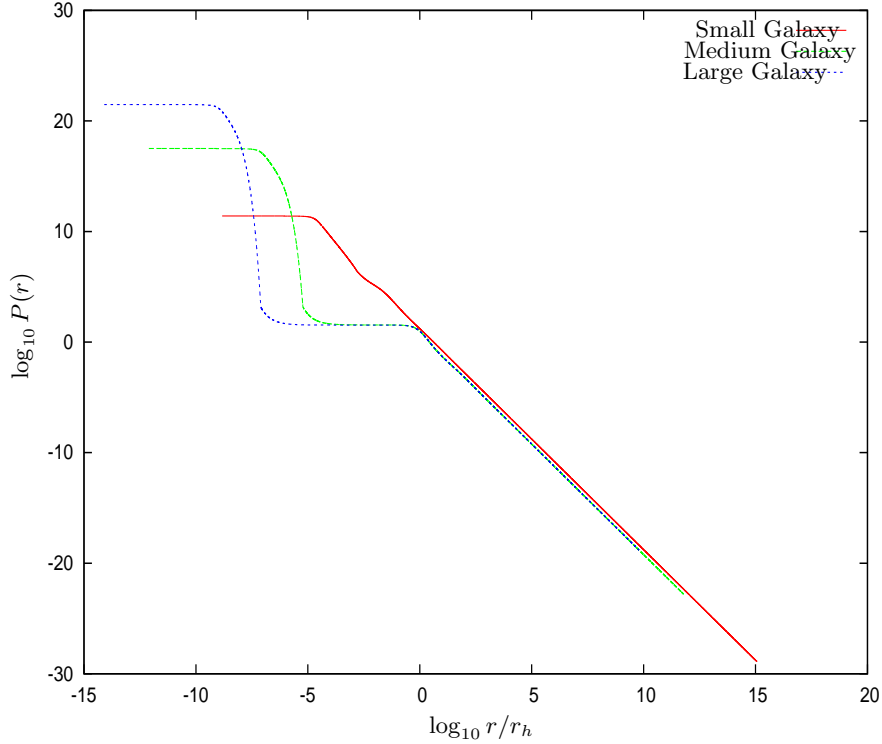


FIG. 13: The logarithm of the local pressure $\log_{10} P(r)$ vs. $\log_{10}(r/r_h)$ for the three galaxy solutions with central SMBH. Notice the huge values of $P(r)$ in the quantum (high density) region $r < r_A$ and its sharp decrease entering the classical (dilute) region $r > r_A$.

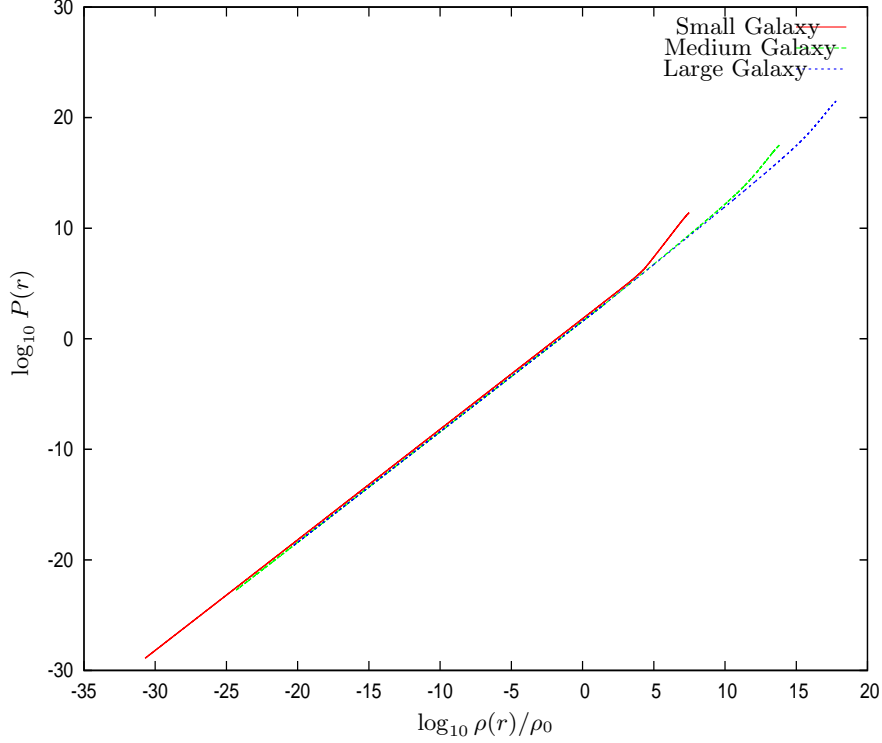


FIG. 14: The obtained equation of state of the galaxy plus central SMBH system: The logarithm of the local pressure $\log_{10} P(r)$ vs. $\log_{10} \rho(r)/\rho_0$. In all the cases we find almost straight lines of unit slope. The equation of state is a perfect gas equation of state in the Boltzmann classical region. In the quantum gas (dense) region the equation of state becomes steeper than the perfect gas. Galaxies with central black holes are in the dilute Boltzmann regime because their halo masses are $M_h > M_h^{min}$ eq.(4.2). This explains the perfect gas equation of state.

class, mass, structure and central SMBH. *Messier 87* is a larger ("supergiant") galaxy within the large class of galaxies we found, and hosting consequently, a bigger central SMBH (M87).

- As explained in the paper, the *central quantum WDM gaz* is relevant for the presence of the obtained central non cusped cores and their correct sizes, and for the presence of the central SMBHs and their realistic mass values without any ad-hoc prescription. Recall for instance Fig. 3 of the paper, which displays the density $\rho(r)$ normalized at the influence radius r_i , vs r/r_h for the three family of galaxy solutions with central SMBHs we found: Large dilute galaxies, intermediate galaxies, and small compact galaxies, covering the different types of galaxies with their central SMBHs. The *Milky Way* is within the Large dilute galaxy class we found with all the characteristic properties of this class: mass, structure and central SMBH, namely $M_{BH} = 4.100 \cdot 10^6 M_\odot$, galaxy mass $M = (0.8 - 1.5) \cdot 10^{12} M_\odot$ and $r_h = 580 + / - 120 kpc$). Notice that in the *quantum WDM gas region* $r < r_A$, the density is constant clearly exhibiting a *plateau* behaviour corresponding to the *quantum macroscopic* Fermi DM gas behaviour in such region. Fig. 3 shows that the local density behaviour is dominated by the black hole for $r \lesssim r_i$. Coherently, for $r_i \lesssim r \lesssim r_h$ the WDM gravitational field dominates over the black hole field and the galaxy core shows up. For medium and large galaxies as the Milky Way the core is seen as a *plateau*. At the same time the chemical potential is negative for $r > r_i > r_A$ and the WDM is a Boltzmann gas in this region.

The first or primary "signatures" are the set of galactic physical magnitudes and structural properties : sizes, masses, cored density profiles and their correct sizes. In particular, *Dwarf* galaxies appear to be a *full quantum macroscopic system*. Dwarf galaxies are really interesting to observe in this respect, as tracers of the quantum keV WDM nature in nearly degenerated states, their temperatures and properties. These are important features all found and provided by the same and one single approach, without tailored prescriptions, and without considering different approaches for each of the different computed magnitudes. Therefore, these are all "signatures" say for this approach.

These results consistently accompass the ones shown in Fig.2 : the derivative of the chemical potential vs. (r/r_h) for the three families of galaxy solutions with central SMBH. For $r \lesssim r_i$ the behaviour is dictated by the central black hole. For $r > r_i$, they are dominated by the WDM and in this region exhibit a similar behaviour to

the Thomas-Fermi galaxy solutions without a central SMBH [9],[10], [11], [12]. For galaxies with central black holes the WDM is in a quantum (highly compact) regime inside the quantum radius r_A . Because r_A is in the parsec scale or smaller [see eqs.(3.8)-(3.10)], the bulk of the WDM is then in the Boltzmann regime eg Fig. 13 and Fig. 14. In the quantum gas (dense) region the equation of state becomes steeper than the perfect gas. Notice the huge values of $P(r)$ in the quantum (high density) region $r < r_A$ and its sharp decrease entering the classical (dilute) region $r > r_A$ all consistent with the other results we found.

- In all the obtained results, and in the Introduction we have carefully compared the results and solutions we obtained in this paper for galaxy systems with a central black hole and without a central black hole. From our results here we recover, in particular, the galaxy structures, the cores of quantum WDM and their right sizes, the velocity dispersions, the scaling relations, the equation of state and the other related results in the absence of black holes we already discussed in our previous works eg Refs [9],[10],[11],[12],[13] in which the careful check for rotation curves, masses, scaling relations, velocities, are in full agreement with observations for the whole set of properties.

Cored density profiles and their right size, halo masses, are in full agreement with the observations. The quantum DM nature in the central regions is *not* an exotic property : It is the quantum nature of the degenerate or nearly degenerate gaz of DM particles. Interaction is fully gravitationnal, namely a self-gravitating and self-consistent WDM gaz. The first or primary " signatures " are therefore the set of galactic physical magnitudes and structural properties: sizes, masses , central cored profiles, velocity distributions, surface density we have found and confronted to real astronomical observations. Other effects as the influence such DM structures could in turn exerce on the propagation of generated gravitational waves, or on the accretion processes, are superimposed effects, or secondary dark matter processes or secondary signatures, a problem which would require to be analysed by its own, and which study is clearly beyond the scope of the present paper which is devoted to the primary dark matter effects, namely the dark matter galactic structures. Those secondary effects as the orbits, diffusion and absorption in the different regions and regimes around the BH and requiring the interaction in propagation with other non dark matter components, as electromagnetic effects and accretion plasmas are not the subject of this paper.

- For the primary objectives of obtaining the galaxy structural magnitudes : eg the realistic astrophysical masses of the galaxies, the realistic SMBH central masses, their sizes, velocities, cored density and pressure profiles, the newtonian treatment is largely enough. Recall that the Thomas-Fermi approach is a statistical many body approach. Near the black hole horizon, there will show up effects of spiraling, orbiting, or a glory effect (180 degrees back scattering) but it does not affect really the properties and magnitudes of the galaxy-black hole system, (and this paper is not devoted to test GR black hole effects, neither horizon nor baryonic effects). The values of the relevant radii here (besides the halo radius): the quantum galaxy radius r_A , the BH influence radius r_i , and the horizon black hole radius r_{BH}^{Schw} are given by eqs.(3.8)-(3.10). The horizon radius is always extremely small with respect to the other radii. For galaxies with virial masses from $10^{16}M_\odot$ to 10^7M_\odot , r_A runs between 0.07 pc to 1.90 pc respectively [as shown in sec. III C], while the horizon radius of the central black hole runs from 10^{-4} pc to 10^{-8} pc for such range of galaxy masses respectively; r_i is larger than r_A : $r_i > r_A \gg r_{BH}^{Schw}$. The important point in order to account for both the realistic galaxy and their central SMBH masses, their sizes, velocities, pressure profiles, density profiles and the core sizes, is the DM nature: keV WDM with its quantum and its relativistic treatment.

Newtonian black holes have many common properties with general relativity black holes, and most importantly, they both have the same size. Recall that Newtonian and post-Newtonian approximation have proven to be remarkably effective even in describing strong-field systems, astrophysical black hole systems (eg binary bhs) inspiraling towards a final merger, (eg Ref [52] and refs therein). Of course, a fully GR treatment is needed to account for a causal space-time structure, central classical space-time curvature singularity, and precise tests of GR, of the horizon or of the "no hair theorems", for which inner orbits at milliparsec (mpc) distances need to be considered but not for the magnitudes of the galactic masses, sizes, and of their central SMBHs. The GR treatment minimally affects the obtained huge mass magnitude values. A high merit of the keV WDM approach is that it accounts naturally (with Dark Matter only) for the realistic astrophysical masses, sizes, density and velocity profiles, rotation curves, equation of state and structural properties of both galaxies and their central SMBHs.

VI. APPENDIX. ANALYTIC EVALUATION OF THE DENSITY AND THE PRESSURE

The density and the pressure were expressed in sec. II in terms of the integrals

$$\begin{aligned}
 I_2(\nu) &= 3 \int_0^\infty y^2 dy \sqrt{1 + \frac{2y^2}{\tau_1}} \Psi_{FD} \left(\tau \left[\sqrt{1 + \frac{2y^2}{\tau_1}} - 1 \right] - \nu \right), \quad \tau_1 \equiv \frac{m}{T_0}, \\
 I_4(\nu) &= 5 \int_0^\infty \frac{y^4 dy}{\sqrt{1 + \frac{2y^2}{\tau_1}}} \Psi_{FD} \left(\tau \left[\sqrt{1 + \frac{2y^2}{\tau_1}} - 1 \right] - \nu \right). \tag{6.1}
 \end{aligned}$$

We evaluate in this Appendix the integrals $I_2(\nu)$ and $I_4(\nu)$ in the limits $\nu \gg 1$ and $\nu \ll -1$ corresponding to the quantum and classical regimes, respectively.

A. The quantum (high density) regime

In order to evaluate the integrals eqs.(6.1) in the $\nu \gg 1$ regime it is convenient to change the integration variable y into z defined as

$$z \equiv \tau \left[\sqrt{1 + \frac{2y^2}{\tau_1}} - 1 \right] - \nu. \tag{6.2}$$

The density integral $I_2(\nu)$ takes then the form

$$I_2(\nu) = \int_{-\nu}^\infty \frac{dz}{e^z + 1} h_2(z + \nu), \quad h_2(\nu) \equiv \frac{3}{2} \left(\frac{\tau_1}{\tau} \right)^{\frac{3}{2}} \left(1 + \frac{\nu}{\tau} \right)^2 \sqrt{\nu \left(1 + \frac{\nu}{2\tau} \right)}. \tag{6.3}$$

It is convenient to split the integral eq.(6.3) into two pieces

$$\int_{-\nu}^\infty = \int_{-\nu}^0 + \int_0^\infty.$$

Eq.(6.3) can then be recasted as

$$I_2(\nu) = \int_0^\nu h_2(z) dz + \int_0^\infty \frac{dz}{e^z + 1} [h_2(\nu + z) - h_2(\nu - z)], \tag{6.4}$$

where small terms of the order $e^{-\nu}$ have been neglected.

The integral in the first term of eq.(6.4) giving the dominant behaviour of $I_2(\nu)$ for $\nu \gg 1$ can be computed in closed form with the result

$$\begin{aligned}
 \int_0^\nu h_2(z) dz &= \frac{3}{8} \left(\frac{\tau_1}{2} \right)^{\frac{3}{2}} \left(1 + \frac{\nu}{\tau} \right) \left[2 \left(1 + \frac{\nu}{\tau} \right)^2 - 1 \right] \sqrt{\frac{\nu}{\tau} \left(2 + \frac{\nu}{\tau} \right)} - \\
 &- \frac{3}{8} \left(\frac{\tau_1}{2} \right)^{\frac{3}{2}} \ln \left[1 + \frac{\nu}{\tau} + \sqrt{\frac{\nu}{\tau} \left(2 + \frac{\nu}{\tau} \right)} \right]. \tag{6.5}
 \end{aligned}$$

Expanding the integrand of the second term of eq.(6.4) in powers of z and integrating term by term yields the subdominant terms of $I_2(\nu)$ for $\nu \gg 1$ as an expansion in inverse powers of ν

$$\begin{aligned}
 &\int_0^\infty \frac{dz}{e^z + 1} [h_2(\nu + z) - h_2(\nu - z)] = \\
 &= \int_0^\infty \frac{dz}{e^z + 1} \left[2z h_2'(\nu) + \frac{z^3}{3} h_2'''(\nu) + \mathcal{O}(z^5) \right] = \frac{\pi^2}{6} h_2'(\nu) + \frac{7\pi^4}{360} h_2'''(\nu) + \dots \tag{6.6}
 \end{aligned}$$

We finally get from eqs.(6.4)-(6.6)

$$\begin{aligned}
I_2(\nu) \stackrel{\nu \gg 1}{\cong} & \frac{3}{8} \left(\frac{\tau_1}{2} \right)^{\frac{3}{2}} (1+q) \left[2(1+q)^2 - 1 \right] \sqrt{q(2+q)} - \\
& - \frac{3}{8} \left(\frac{\tau_1}{2} \right)^{\frac{3}{2}} \ln \left[1+q + \sqrt{q(2+q)} \right] - \frac{\pi^2}{8\sqrt{\nu}} \left(\frac{\tau_1}{\tau} \right)^{\frac{3}{2}} \frac{(1+q)(3q^2+6q+1)}{\sqrt{1+\frac{q}{2}}} + \\
& + \frac{7\pi^4}{640\nu^{\frac{5}{2}}} \left(\frac{\tau_1}{\tau} \right)^{\frac{3}{2}} (2q^4+8q^3+7q^2-2q+1) \frac{(1+q)}{\left(1+\frac{q}{2}\right)^{\frac{5}{2}}}, \quad q \equiv \frac{\nu}{\tau}
\end{aligned}$$

where we used eq.(6.3).

The pressure integral $I_4(\nu)$ can be treated analogously to the density integral $I_2(\nu)$ using the integration variable z eq.(6.2)

$$I_4(\nu) = \int_{-\nu}^{\infty} \frac{dz}{e^z+1} h_4(z+\nu) \quad , \quad h_4(\nu) \equiv \frac{5}{2} \left(\frac{\tau_1}{\tau} \right)^{\frac{3}{2}} \left[\nu \left(1 + \frac{\nu}{2\tau} \right) \right]^{\frac{3}{2}}. \quad (6.7)$$

Proceeding as above for $I_2(\nu)$ we obtain

$$I_4(\nu) = \int_0^{\nu} h_4(z) dz + \int_0^{\infty} \frac{dz}{e^z+1} [h_4(\nu+z) - h_4(\nu-z)], \quad (6.8)$$

where small terms of the order $e^{-\nu}$ have been neglected and the dominant contribution becomes

$$\begin{aligned}
\int_0^{\nu} h_4(z) dz &= \frac{5}{32\sqrt{2}} \tau \tau_1^{\frac{3}{2}} \left[(2q^2+4q-3)(q+1)\sqrt{q(q+2)} \right] + \\
& + \frac{15}{32\sqrt{2}} \tau \tau_1^{\frac{3}{2}} \ln \left[(1+q)^2 + \sqrt{q(2+q)} \right], \quad q \equiv \frac{\nu}{\tau}.
\end{aligned} \quad (6.9)$$

The subdominant terms of $I_4(\nu)$ for $\nu \gg 1$ follow by expanding as in eq.(6.6) and we finally get from eqs.(6.8)-(6.9)

$$\begin{aligned}
I_4(\nu) \stackrel{\nu \gg 1}{\cong} & \frac{5}{32\sqrt{2}} \tau \tau_1^{\frac{3}{2}} \left[(2q^2+4q-3)(q+1)\sqrt{q(q+2)} \right] + \\
& + \frac{15}{32\sqrt{2}} \tau \tau_1^{\frac{3}{2}} \ln \left[(1+q)^2 + \sqrt{q(2+q)} \right] + \frac{5\pi^2}{8\sqrt{2}} \left(\frac{\tau_1}{\tau} \right)^{\frac{3}{2}} \sqrt{\nu(q+2)}(q+1) + \\
& + \frac{7\pi^4}{96\sqrt{2}} \left(\frac{\tau_1}{\tau} \right)^{\frac{3}{2}} \frac{(q+1)(2q^2+4q-1)}{[\nu(q+2)]^{\frac{3}{2}}}.
\end{aligned} \quad (6.10)$$

B. The classical Boltzmann regime

In the classical Boltzmann regime $\nu \ll -1$ and because $e^{\nu} \ll 1$, the Fermi–Dirac distribution can be approximated by the exponent of the Boltzmann distribution

$$\frac{1}{\left[e^{\left(\tau \sqrt{1 + \frac{2y^2}{\tau_1}} - \tau - \nu \right)} + 1 \right]} = e^{\nu+\tau} e^{-\tau \sqrt{1 + \frac{2y^2}{\tau_1}}} + \mathcal{O}(e^{2\nu}) \quad (6.11)$$

Inserting eq.(6.11) into eq.(6.1) for $I_2(\nu)$ yields

$$\begin{aligned} I_2(\nu) &\stackrel{\nu \ll -1}{\approx} 3 \exp(\nu + \tau) \int_0^\infty y^2 dy \sqrt{1 + \frac{2y^2}{\tau_1}} e^{-\tau \sqrt{1 + \frac{2y^2}{\tau_1}}} + \mathcal{O}(e^{2\nu}) = \\ &= 3 \left(\frac{\tau_1}{8}\right)^{\frac{3}{2}} e^{\nu+\tau} [K_4(\tau) - K_0(\tau)] + \mathcal{O}(e^{2\nu}) , \end{aligned} \quad (6.12)$$

where $K_n(\tau)$ stands for the Bessel functions of imaginary argument $n = 2, 4$.

Because $\tau \gg 1$, eq.(6.12) can be approximated as

$$I_2(\nu) \stackrel{\nu \ll -1, \tau \gg 1}{\approx} \frac{3}{4} \sqrt{\pi} e^\nu \left(\frac{\tau_1}{\tau}\right)^{\frac{3}{2}} \left[1 + \frac{27}{8\tau} + \mathcal{O}\left(\frac{1}{\tau^2}\right)\right] + \mathcal{O}(e^{2\nu}) . \quad (6.13)$$

The pressure integral $I_4(\nu)$ can be computed analogously by inserting eq.(6.11) into eq.(6.1) for $I_4(\nu)$

$$\begin{aligned} I_4(\nu) &\stackrel{\nu \ll -1}{\approx} 5 \exp(\nu + \tau) \int_0^\infty \frac{y^4 dy}{\sqrt{1 + \frac{2y^2}{\tau_1}}} e^{-\tau \sqrt{1 + \frac{2y^2}{\tau_1}}} + \mathcal{O}(e^{2\nu}) = \\ &= \frac{15}{4\sqrt{2}} \frac{\tau_1^{\frac{5}{2}}}{\tau^2} e^{\nu+\tau} K_2(\tau) + \mathcal{O}(e^{2\nu}) . \end{aligned} \quad (6.14)$$

For $\tau \gg 1$ we obtain the simpler expression:

$$I_4(\nu) \stackrel{\nu \ll -1, \tau \gg 1}{\approx} \frac{15}{8} \sqrt{\pi} \left(\frac{\tau_1}{\tau}\right)^{\frac{5}{2}} e^\nu \left[1 + \frac{15}{8\tau} + \mathcal{O}\left(\frac{1}{\tau^2}\right)\right] + \mathcal{O}(e^{2\nu}) . \quad (6.15)$$

-
- [1] H. J. de Vega, N. G. Sánchez, MNRAS. **404**, 885 (2010).
 - [2] Cosmic Frontiers, H. J. de Vega, N. G. Sanchez arXiv:1304.0759.
 - [3] P.L. Biermann, H.J. de Vega and N.G. Sanchez, Highlights and Conclusions of the Chalonge Meudon Workshop 2012, arXiv:1305.7452.
 - [4] H. J. de Vega, M.C. Falvela and N. G. Sanchez, Highlights and Conclusions of the Chalonge 16th Paris Cosmology Colloquium 2012, arXiv:1307.1847.
 - [5] H. J. de Vega and N. G. Sanchez, Phys. Rev. D85, 043516, (2012) and Phys. Rev. D85,043517, (2012).
 - [6] C. Destri, H. J. de Vega and N. G. Sanchez, Phys. Rev. D88, 083512 (2013).
 - [7] H. J. de Vega, O. Moreno, E. M. de Guerra, M. Ramon Medrano, and N. G. Sanchez, Nucl. Phys. B866, 177 (2013).
 - [8] L. Lello, D. Boyanovsky, Phys. Rev. D91, 063502 (2015).
 - [9] C. Destri, H. J. de Vega, N. G. Sanchez, New Astronomy **22**, 39 (2013).
 - [10] C. Destri, H. J. de Vega, N. G. Sanchez, Astrop. Phys., **46**, 14 (2013).
 - [11] H. J. de Vega, P. Salucci, N. G. Sanchez, MNRAS, 442, 2717 (2014).
 - [12] H. J. de Vega, N. G. Sánchez, The European Physical Journal C, **77** (2), 1-19 (2017).
 - [13] H. J. de Vega, N. G. Sánchez, Int. J. Mod. Phys. **A 31**, 1650073 (2016).
 - [14] N. Menci, N. G. Sanchez, M. Castellano, A. Grazian, ApJ, 818, 90 (2016).
 - [15] A White Paper on keV Sterile Neutrino Dark Matter, M. Drewes, T. Lasserre, A. Merle, S. Mertens, R. Adhikari et al., JCAP 01, 025 (2017).
 - [16] J.A. Dror, G. Elor, and R. McGehee, Phys. Rev. Lett. 124, 181301, (2020).
 - [17] A. Rudakovskiy, A. Mesinger, D. Savchenko, N. Gillet, MNRAS 507, 3046, (2021).
 - [18] *Universe*, this Special Issue keV Warm Dark Matter in Agreement with Observations in tribute to Hector de Vega, (2021) and the papers therein.
 - [19] P. Colín, O. Valenzuela, V. Avila-Reese, Ap J, 542, 622 (2000).
 - [20] J. Sommer-Larsen, A. Dolgov, Ap J, 551, 608 (2001).
 - [21] L. Gao and T. Theuns, Science, 317, 1527 (2007).
 - [22] A. V. Tikhonov et al., MNRAS, 399, 1611 (2009).
 - [23] J. Zavala et al., Ap J, 700, 1779 (2009).

- [24] E. Papastergis et al., *Ap J*, 739, 38 (2011).
- [25] M. R. Lovell et al., *MNRAS*, 420, 2318 (2012).
- [26] M. R. Lovell et al. *MNRAS*, 439, 300 (2014).
- [27] Anderhalden D. et al., *JCAP*, 03, 014 (2013).
- [28] R. F. G. Wyse, G. Gilmore, *IAU Symposium*, Vol. 244, p. 44-52 (2007), arXiv:0708.1492. J. van Eymeren et al. *A & A* 505, 1-20 (2009). W. J. G. de Blok, *Advances in Astronomy*, vol. 2010, pp. 1-15, (2010). P. Salucci, Ch. Frigerio Martins, *EAS Publications Series*, 36, 2009, 133-140.
- [29] G. Gilmore et al., *Ap J*, 663, 948 (2007).
- [30] M. Walker, J. Peñarrubia, *Ap. J.* 742, 20 (2011).
- [31] M. Spano et al., *MNRAS*, 383, 297 (2008).
- [32] F. Donato et al., *MNRAS* **397**, 1169 (2009).
- [33] J Kormendy, K C Freeman, *IAU Symposium*, Sydney, 220, 377 (2004), arXiv:astro-ph/0407321.
- [34] V. Avila-Reese et al., *Ap J*, 559, 516 (2001).
- [35] P. Colín, O. Valenzuela, V. Avila-Reese, *Ap J*, 673, 203 (2008).
- [36] J. Viñas, E. Salvador-Solé, A. Manrique, *MNRAS* 424, L6 (2012).
- [37] A. Macciò, S. Paduroiu, D. Anderhalden, A. Schneider, B. Moore, *MNRAS* 424, 1105 (2012).
- [38] L D Landau and E M Lifshits, *Statistical Mechanics*, Elsevier, Oxford, 1980.
- [39] F. Munyaneza, P. L. Biermann, *A & A*, 458, L9 (2006). P. H. Chavanis, *Phys. Rev.* **E65**, 056123 (2002), P. H. Chavanis, *Int. J. Mod. Phys. B*20, 3113 (2006).
- [40] J. Binney and S. Tremaine, 'Galactic Dynamics', 2nd. edition, Princeton Univ. Press, 2008.
- [41] H. J. de Vega, N. G. Sánchez, *Nuclear Physics B* **625**, 409 and 460 (2002).
- [42] D. Boyanovsky, H. J. de Vega and N. G. Sanchez, *Phys. Rev. D* 77, 043518, (2008) and *Phys. Rev. D* 78, 063546, (2008).
- [43] H. J. de Vega, P. Salucci, N. G. Sanchez, *New Astronomy* **17**, 653 (2012).
- [44] A. W. McConnachie, *AJ*, 144, 4 (2012).
- [45] N. Menci, F. Fiore, A. Lamastra, *ApJ*, 766, 110 (2013).
- [46] A. M. Nierenberg et al. *ApJ* 772, 146 (2013).
- [47] F. Pacucci et al., *MNRAS Letters* 435L, 53 (2013).
- [48] P. Salucci et al. *MNRAS* **378**, 41 (2007).
- [49] J. D. Simon, M. Geha, *Ap J*, 670, 313 (2007) and references therein. J. D. Simon et al., *Ap. J.* 733, 46 (2011) and references therein. J. Wolf et al., *MNRAS*, 406, 1220 (2010) and references therein. J. P. Brodie et al., *AJ*, 142, 199 (2011). G. D. Martinez et al., *Ap J*, 738, 55 (2011). B. Willman and J. Strader, *AJ*, 144, 76 (2012).
- [50] S. Shao et al. *MNRAS*, 430, 2346 (2013).
- [51] C. R. Watson, Z. Li, N. Polley, *JCAP* 03, 018 (2012).
- [52] Clifford M. Will, *Theory and Experiment in Gravitational Physics*, Cambridge University Press, UK, 2nd Ed. (2018).